Annu. Rev. Astron. Astrophys. 2000. 38:667–715

THE HUBBLE DEEP FIELDS

Henry C. Ferguson, Mark Dickinson, and Robert Williams
Space Telescope Science Institute , Baltimore, MD 21218; e-mail: ferguson@stsci.edu

Key Words cosmology observations, galaxy evolution, galaxy formation, galaxy photometry, surveys

■ **Abstract** The Hubble space telescope observations of the northern Hubble deep field, and more recently its counterpart in the south, provide detections and photometry for stars and field galaxies to the faintest levels currently achievable, reaching magnitudes $V \sim 30$. Since 1995, the northern Hubble deep field has been the focus of deep surveys at nearly all wavelengths. These observations have revealed many properties of high redshift galaxies and have contributed to important data on the stellar mass function in the Galactic halo.

1. INTRODUCTION

Deep surveys have a long history in optical astronomy. Indeed, nearly every telescope ever built has at some point in its lifetime been pushed to its practical limit for source detection. An important historical motivation for such surveys has been the desire to test cosmological models via the classical number–magnitude and angular-diameter–magnitude relations (Sandage, 1961, 1988). However, interpretation has always been hampered by the difficulty of disentangling the effects of galaxy selection and evolution from the effects of cosmic geometry. The modern era of deep surveys in optical astronomy began with the advent of CCD detectors, which allowed 4-m telescopes to reach to nearly the confusion limit allowed by the point spread function (Tyson, 1988). These images revealed a high surface density of faint, blue galaxies, and the combination of their number–magnitude relation, number–redshift relation, and angular correlation function was difficult to reconcile with the critical-density universe ($\Omega_M = \Omega_{\rm tot} = 1$) that seemed at the time to be a robust expectation from inflationary models (Kron 1980; Fukugita et al 1990, Guiderdoni & Rocca-Volmerange, 1990; Efstathiou et al 1991).

Prior to launch, simulations based on fairly conservative assumptions suggested that the Hubble space telescope (HST) would not provide an overwhelming advantage over ground-based telescopes for studies of distant galaxies (Bahcall et al 1990):

> Our results show that the most sensitive exposures achieved so far from the ground reveal more galaxies per unit area than will be seen by planned HST observations unless galaxy sizes decrease with the maximum rate consistent with ground-based observations. In this, the most favorable case for HST, the space exposures will show almost as many galaxy images as have been observed so far in the most sensitive ground-based data.

It was apparent from the images returned immediately after the HST refurbishment in 1993 that distant galaxies had substantially higher surface brightnesses than predicted by such simulations (Dressler et al 1994; Dickinson, 1995). Despite the pessimistic predictions, extensive field galaxy surveys were always a top priority for HST, and large amounts of observing time were awarded to deep, pointed surveys and to the medium-deep survey (Griffiths et al 1996). These observations provided valuable information on galaxy scale lengths and morphologies, on the evolution of clustering and the galaxy merger rate, and on the presence of unusual types of galaxies (Mutz et al 1994; Schade et al 1995a; Cowie et al 1995a; Griffiths et al 1996). In this context, the idea of using the HST to do an ambitious deep field survey began to look quite attractive, and was eventually adopted as one of the primary uses of the HST director's discretionary time.

1.1 This Review

The Hubble deep fields north and south (HDF-N and HDF-S, respectively) are by now undoubtedly among the most "data rich" portions of the celestial sphere. The task of reviewing progress is complicated by the fact that much of the supporting data are still being gathered, and by the wide range of uses that have been found for the HDF. It is not practical to provide a comprehensive review of all HDF-related research in a single review article. Instead we have chosen to divide the review into two parts. The first part discusses the data, both from HST and from other facilities, and summarizes measurements and phenomenology of the sources found in the field. The second part focuses specifically on distant galaxies, and attempts to provide a critical view of what the HDF has, and has not, taught us about galaxy evolution. Ferguson (1998a) has reviewed the HDF with a different focus, and the series of papers in the 1996 Herstmonceux conference and the 1997 STScI May Symposium provide a broad summary of the overall field (Tanvir et al 1996; Livio et al 1997). Throughout this review, unless explicitly stated otherwise, we adopt cosmological parameters Ω_M, Ω_Λ, $\Omega_{\rm tot} = 0.3, 0.7, 1.0$ and $H_0 = 65\,{\rm km\,s^{-1}}$ Mpc^{-1}. Where catalog numbers of galaxies are mentioned, they refer to those in Williams et al (1996).

2. PART 1: Observations, Measurements, and Phenomenology

The HDFs were carefully selected to be free of bright stars, radio sources, nearby galaxies, etc., and to have low Galactic extinction. The HDF-S selection criteria included finding a quasi-stellar object (QSO) that would be suitable for studies of absorption lines along the line of sight. Field selection was limited to the

"continuous viewing zone" around $\delta = \pm 62^\circ$, because these declinations allow HST to observe, at suitable orbit phases, without interference by earth occultations. Apart from these criteria, the HDFs are typical high-galactic-latitude fields; the statistics of field galaxies or faint Galactic stars should be free from a priori biases. The HDF-N observations were taken in December 1995 and the HDF-S in October 1998. Both were reduced and released for study within 6 weeks of the observations. Many groups followed suit and made data from follow-up observations publicly available through the world wide web.

Details of the HST observations are set out in Williams et al (1996), for HDF-N and in a series of papers for the southern field (Williams et al 2000; Ferguson et al 2000; Gardner et al 2000; Casertano et al 2000; Fruchter et al 2000; Lucas et al 2000). The HDF-N observations primarily used the WFPC2 camera, whereas the southern observations also took parallel observations with the new instruments installed in 1997: the near-infrared camera and multi-object spectrograph (NICMOS) and the space telescope imaging spectrograph (STIS). The area of sky covered by the observations is small: 5.3 arcmin^2 in the case of WFPC2 and 0.7 arcmin^2 in the case of STIS and NICMOS for HDF-S. The WFPC2 field subtends about 4.6 Mpc at $z \sim 3$ (comoving, for Ω_M, Ω_Λ, $\Omega_{\rm tot} = 0.3, 0.7, 1.0$). This angular size is small relative to scales relevant for large-scale structure.

The WFPC2 observing strategy was driven partly by the desire to identify high-redshift galaxies via the Lyman-break technique (Guhathakurta et al 1990; Steidel et al 1996), and partly by considerations involving scattered light within HST (Williams et al 1996). The images were taken in four very broad bandpasses (F300W, F450W, F606W, and F814W), spanning wavelengths from 2500 to 9000 Å. Although filter bandpasses and zeropoints are well calibrated,[1] no standard photometric system has emerged for the HDF. In this review, we use the notation U_{300}, B_{450}, V_{606} and I_{814} to denote magnitudes in the HST passbands on the AB system (Oke, 1974). On this system $m(AB) = -2.5 \log f_\nu({\rm nJy}) + 31.4$. Where we drop the subscript, magnitudes are typically on the Johnson-Cousins system, as defined by Landolt (1973, 1983, 1992a,b) and as calibrated for WFPC2 by Holtzman et al (1995); however we have not attempted to homogenize the different color corrections and photometric zeropoints adopted by different authors.

During the observations, the telescope pointing direction was shifted ("dithered") frequently, so that the images fell on different detector pixels. The final images were thus nearly completely free of detector blemishes, and were sampled at significantly higher resolution than the original pixel sizes of the detectors. The technique of variable pixel linear reconstruction ("drizzling") (Fruchter & Hook 1997) was developed for the HDF and is now in widespread use.

[1]None of the analyses to date have corrected for the WFPC2 charge-transfer inefficiency (CTE; Whitmore et al. 1999). This is likely to be a small correction $\lesssim$5% for the F450W, F606W, and F814W bands. However, because of the low background in the F300W band, the correction could be significantly larger.

TABLE 1 Census of objects in the central HDF-N

Number	Type of source
∼3000	Galaxies at U_{300}, B_{450}, V_{606}, I_{814}
∼1700	Galaxies at J_{110}, H_{160}
∼300	Galaxies at K
9	Galaxies at 3.2 μm
∼50	Galaxies at 6.7 or 15 μ
∼5	Sources at 850 μm
0	Sources at 450 μm or 2800 μm
6	X-ray sources
∼16	Sources at 8.5 GHz
∼150	Measured redshifts
∼30	Galaxies with spectroscopic $z > 2$
<20	Main-sequence stars to $I = 26.3$
∼2	Supernovae
0−1	Strong gravitational lenses

Both HDF campaigns included a series of shallow "flanking field" observations surrounding the central WFPC2 field. These have been used extensively to support ground-based spectroscopic follow-up surveys. Since 1995, HDF-N has also been the target of additional HST observations. Very deep NICMOS imaging and spectroscopy were carried out on a small portion of the field by Thompson et al (1999). Dickinson et al (2000b) took shallower NICMOS exposures to make a complete map of the WFPC2 field. A second epoch set of WFPC2 observations were obtained in 1997, 2 years after the initial HDF-N campaign (Gilliland et al 1999). STIS ultraviolet (UV) imaging of the field is in progress, and a third epoch with WFPC2 is scheduled.

Table 1 gives a rough indication of the different types of sources found in the HDF-N. Since 1995, the field has been imaged at wavelengths ranging from 1×10^{-3} μm (ROSAT) to 2×10^{5} μm (MERLIN and VLA), with varying sensitivities, angular resolutions, and fields of view. Not all of the data have been published or made public, but a large fraction has, and it forms the basis for much of the work reviewed here. Links to the growing database of observations for HDF-S and HDF-N are maintained on the HDF world wide web sites at STScI.

3. STARS

The nature of the faint stellar component of the Galaxy is critical to determining the stellar luminosity function and the composition of halo dark matter. In spite of the small angular sizes of the HDFs, their depth enables detection of low-luminosity

objects to large distances. If the halo dark-matter is mostly composed of low-mass stars, there should be several in the HDF (Kawaler, 1996, 1998). Although HST resolution permits star-galaxy separation down to much fainter levels than ground-based observations, many distant galaxies also appear nearly point-like. Color criteria are effective at identifying likely red subdwarfs, but for $I_{814} > 25$ and $V_{606} - I_{814} < 1$ the possibility of galaxy contamination becomes significant. The counts of red main-sequence stars have been compared with galactic models by Flynn et al (1996), Elson et al (1996) and Mendez et al (1996). More detailed results have subsequently emerged from studies that have combined the HDF-N with other HST images to increase the sky coverage (Gould et al 1996, 1997; Reid et al 1996; Mendez & Guzman, 1997; Kerins, 1997; Chabrier & Mera, 1997). A general conclusion is that hydrogen-burning stars with masses less than 0.3 $M_\odot$ account for less than 1% of the total mass of the Galactic halo. The overall HST database indicates that the Galactic disk luminosity function experiences a decided downturn for magnitudes fainter than $M_v = 12 (M \lesssim 0.2\ M_\odot)$. For the halo, the constraints on the luminosity function are not as good because of the limited sky coverage. However, the luminosity function clearly cannot turn up by the amount it would need for main-sequence stars to be an important constituent of halo dark matter.

In addition to the nine or so candidate red dwarfs in the HDF-N, to a limiting magnitude of $I = 28$ the field has about 50 unresolved objects with relatively blue colors. Although in principle these could be young hot white dwarfs (WDs), this possibility has appeared unlikely, as the lack of brighter point sources with similar colors would require all to be at very large distances, greater than 10 kpc away. However, recent work by Hansen (1998, 1999) has shown that at low metallicity, molecular hydrogen opacity causes the oldest, lowest luminosity WDs to become blue as they cool. Harris et al (1999) have recently discovered such an object in the Luyten proper motion survey. This result changes the way in which colors should be used to discriminate faint point-like sources in the HDFs, and may lead to the reclassification of some faint galaxies as WDs.

Proper motions are an unambiguous way to distinguish between galactic stars and galaxies. The HDFs serve as excellent first-epoch data for detection of changes in position or brightness for any objects. A second-epoch set of images of the HDF-N were obtained 2 years after the initial HDF-N campaign (Gilliland et al 1999), and were analyzed by Ibata et al (1999) to search for object motion in the images. Of 40 identified point sources with $I > 28$, five were found to have proper motions that were $>3\sigma$ above the measurement uncertainty ($\sim$10 mas year^{-1}), with two of the objects having proper motions exceeding 25 mas/yr and the remaining three near the detection limit. The five objects are all faint ($I \sim 28$) and of neutral color ($V - I < 0.9$), and realistic velocities require that they have distances $d < 2$ kpc. Although only a very small fraction of the total sources in the HDF-N, these objects represent a large increase over the number of stars expected from standard models of the Galaxy, which predict less than one star in the range $27 < V < 29$ with $V - I < 1.0$.

Separate evidence may be emerging that is consistent with the identification of faint blue stars in the HDFs. The HDF-S ($l = 328$, $b = -49$) points closer to the Galactic center than HDF-N ($l = 126$, $b = 55$), and hence samples a larger path length through the Galactic halo. There should be more stars in HDF-S than in HDF-N. Mendez & Minniti (1999) found roughly double the number of blue point-like sources in the HDF-S than its northern counterpart (Figure 1). This supports the hypothesis that a significant fraction of these sources are stars. A number of these stars are too faint and too blue to be on the main sequence, and could represent the old, low luminosity, blueish halo WDs proposed by Hansen (1998).

Although these developments are exciting, the evidence is far from compelling. The sources identified by Mendez & Minniti (1999) are brighter than those found to have proper motions by Ibata et al (1999). The two studies thus appear to be inconsistent, in that the closer WDs ought to have larger proper motions. Also, the enhancement in faint blue point-like objects in HDF-S relative to HDF-N is sensitive to the magnitude limit chosen. If Mendez & Minniti (1999) had included objects down to $I = 29$ in their sample, they would have found more objects in HDF-N than in HDF-S (Figure 1).

Although still very tentative, the identification of WDs in the HDFs is potentially extremely important. The results of the MACHO project (Alcock et al 1997) suggest that a substantial fraction of the halo mass is due to objects with WD masses (although this is not a unique interpretation of the microlensing statistics) (Sahu 1994). If WDs do contribute significantly to the halo mass, then the early stellar population of the halo must have formed with a peculiar initial mass function (IMF) (Reid et al 1996) deficient in both high-mass stars [to avoid over-enrichment of the halo by metals from supernovae (SN) and planetary nebulae] and low mass stars, (because stars with $M < 0.8\ M_{\odot}$ would still be on the main sequence today). The presence or absence of WDs in deep fields will become more definite within the next few years via forthcoming third-epoch proper motion measurements.

3.1 Supernova Events

An estimate of the SN rate at high redshift can provide important constraints on the star-formation history of galaxies and on models for SN progenitors (Pain et al 1996; Madau et al 1998; Ruiz-Lapuente & Canal, 1998). Gilliland & Phillips (1998) took second-epoch WFPC2 observations of the HDF-N field in December 1997 and reported two SN detections, at $I = 26.0$ and 27.0. Mannucci & Ferrara (1999) report a very faint detection, at $I = 28.5$ of an object that brightened by 1 mag in 5 days in the original HDF-N images. The number of SNe expected in a single epoch of HDF-N observations is 0.5–1 (Gilliland et al 1999), consistent with the number of detections. The advanced camera for surveys (ACS) will provide substantial benefits for future SN searches, because it will have roughly twice the solid angle at five times the sensitivity of WFPC2. Based on the HDF numbers, a survey of 12 ACS fields to HDF *I*-band depth should identify roughly 25 SNe and would cost $\sim$100 orbits.

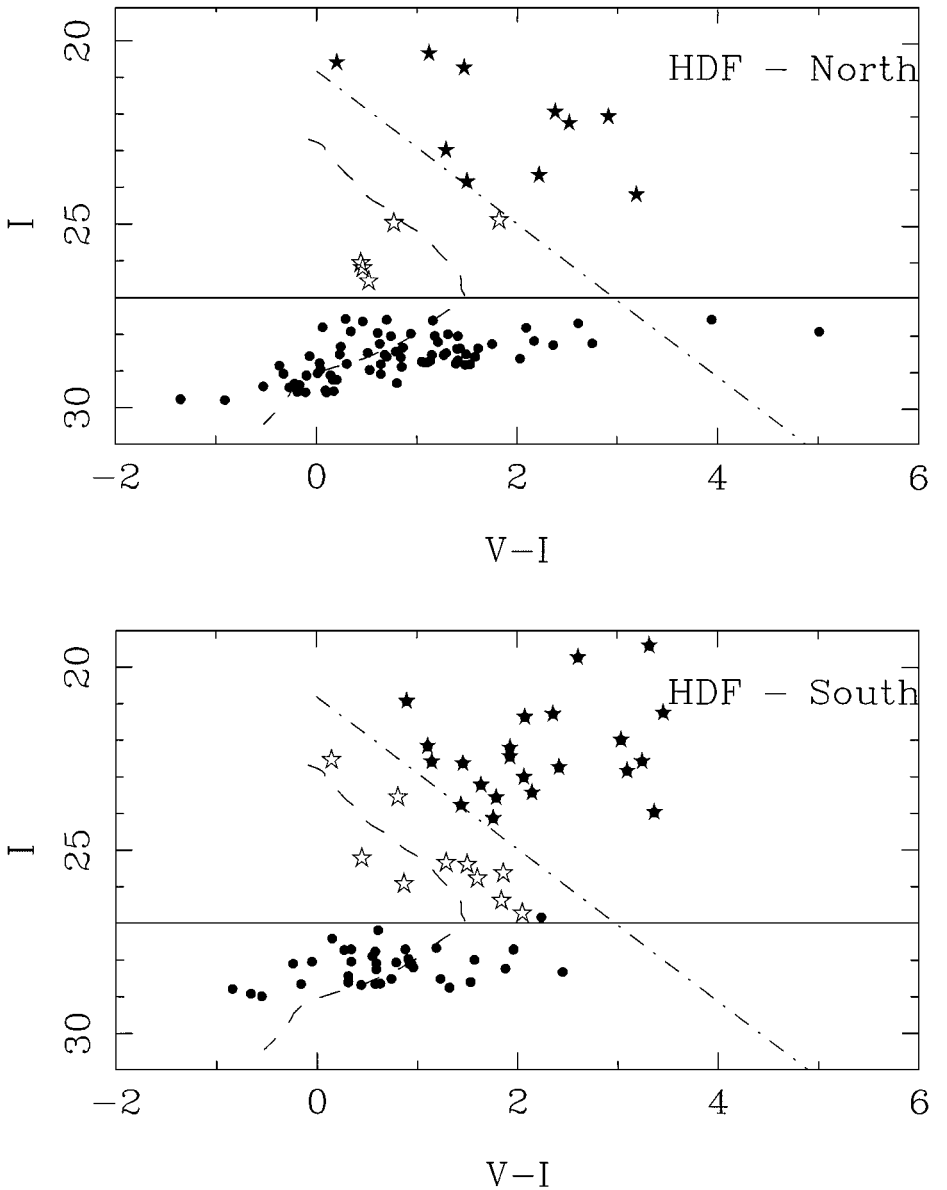

Figure 1 Color-magnitude diagrams for point sources in the HDF-N and HDF-S. The dash-dot line represents locus of disk M-dwarfs at a distance of 8 kpc, with solid star symbols representing main-sequence disk and halo stars. The horizontal line represents the (15σ) detection limit of $I =$ 27 magnitude, and filled circles below that line are Galactic stars and unresolved distant galaxies. The open star symbols represent point sources which are too faint to be on the main sequence at any reasonable distance, and which may be white dwarfs. The dashed line is the 0.6 $M_{\odot}$ WD cooling track from Hansen (1999) for a distance of 2 kpc. (adapted from Mendez & Minniti 2000)

4. GALAXIES

The HDFs are exquisitely deep and sharp images, detecting thousands of objects distributed throughout the observable universe, but they are also *very small* fields of view, and each is only one sightline. Figure 2 illustrates some parameters relevant for studying galaxy evolution with a single HDF. The total co-moving volume out to redshift z has been scaled (*top panel*) by the present-day normalization of the galaxy luminosity function ϕ^*. This gives a rough measure of the number of

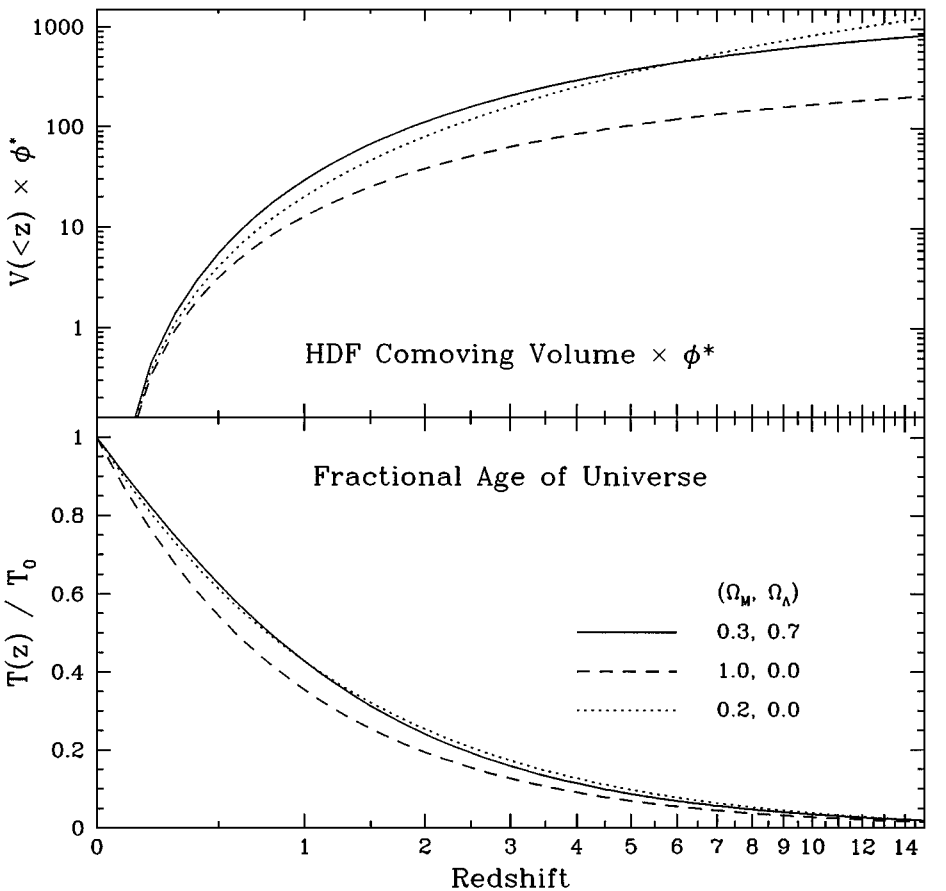

Figure 2 An illustration of volume and time in the HDF. At top, for the 5 arcmin^2 WFPC2 field of view, the co-moving volume out to redshift z is plotted for several cosmologies, scaled by the present-day normalization of the galaxy luminosity function (ϕ^*, here taken to be 0.0166) h^3 Mpc^{-3}, from Gardner et al (1997). This gives a rough measure of the number of "L^*-volumes" out to that redshift. At bottom, the fractional age of the universe versus redshift is shown. Most of cosmic time passes at low redshifts, where the HDF volume is very small.

"L^*volumes" out to z, i.e. approximately the number of L^* galaxies expected in that volume, or at high redshift the number of L^* galaxies that the "proto-galaxies" found there will someday become. At $z < 1$, this number is ∼10–30 depending on the cosmology: very few high-luminosity galaxies are expected (or found, for that matter), and even purely Poissonian variations introduce large uncertainties in any statistical conclusions that can be derived from them. Given real galaxy clustering, these uncertainties are still greater. As an example, ∼24% of the total rest-frame 6500 Å luminosity summed over all HDF-N galaxies out to $z = 1.1$ comes from just four galaxies: two in a redshift "spike" at $z = 0.96$ and two in another spike at $z = 1.02$. The safest use (statistically) for the HDF at $z < 1$ is thus to study the vastly more numerous, low-luminosity galaxies. This caution similarly applies to clustering studies. The angular correlation functions derived from the $z \lesssim 1$ sample primarily refer to low-luminosity galaxies, whereas those at higher z refer to higher luminosities. Clustering variation with luminosity (or mass) can mimic evolution.

At high redshift, the HDF volume is large (especially for the open and Λ cosmologies), and thus is more likely to provide a fair sample of objects.[2] For $(\Omega_M, \Omega_\Lambda) = (0.3, 0.7)$ there is ∼20 × more volume at $2 < z < 10$ than at $0 < z < 1$, and the likelihood of finding even moderately rare objects becomes significant. There is, however, little *time* out at high redshift: Most of cosmic history takes place at $z < 1$ (Figure 2, *bottom*).

4.1 Galaxy Colors and Morphology

One of the long-term goals of faint galaxy surveys is to chart the origin and history of the Hubble sequence. In the nearby universe, most galaxies near the knee (L^*) of the Schechter (1976) luminosity function are elliptical, lenticular, or spiral galaxies. Although such normal galaxies dominate the integrated mass and luminosity density at $z = 0$, lower-luminosity dwarf irregular and dwarf elliptical galaxies dominate by number. High-luminosity peculiar or interacting galaxies are relatively rare, constituting 2–7% of the population in the local volume $v < 500$ km s^{-1} (Karachentsev & Makarov, 1997).

Attempts to extend galaxy classification and quantitative surface photometry to magnitudes fainter than $V \sim 20$ were pioneered by the medium deep survey (MDS) team (Casertano et al 1995; Driver et al 1995; Glazebrook et al 1995). By the time of the HDF observations it was clear from such analysis that the galaxy population at $I \sim 23$ contained a larger fraction of irregular or peculiar galaxies than would be expected from a simple extrapolation of galaxy populations in the local universe. The HDF in particular has spurred considerable effort toward quantifying galaxy morphologies using a wide variety of methods, including traditional Hubble-sequence classification, concentration and asymmetry parameters, neural

[2]Even at high redshift, however, uncertainties due to clustering (cf. Adelberger et al 1998) need to be kept in mind when analyzing one or two sightlines like the HDFs.

network classification, and bulge/disk decomposition via profile fitting (van den Bergh et al 1996; Abraham et al 1996; Odewahn et al 1996; Marleau & Simard, 1998). The classifications derived by different methods are not always in agreement. There are many considerations to take into account when analyzing HST morphologies, including the behavior of the classifier with signal-to-noise and image size (few HDF galaxies have more than 100 independent resolution elements within an area defined by some isophote reasonably exceeding the sky noise level), and redshift effects both on surface brightness (the $(1+z)^4$ Tolman dimming) and on rest-frame wavelengths sampled by a given image. Abraham et al (1996) used the HDF to extend the MDS results to $I = 25$. They measured the concentration and asymmetry of the galaxy images, and also classified each galaxy by eye, finding that at $I = 25$, irregular/merging/peculiar systems comprise 40% of all galaxies. The progressive shifting of UV wavelengths into the optical for higher redshift galaxies may account for part of the trend (Bohlin et al 1991; Giavalisco et al 1996; Hibbard & Vacca, 1997), but according to Abraham (1997) and Abraham et al (1999a) this is not the dominant effect (see also Section 5.2 below).

NICMOS observations (Teplitz et al 1998; Thompson et al 1999; Dickinson et al 2000a; Fruchter et al 2000), which sample the redshifted rest-frame optical light out to nearly $z \sim 3$, further confirm that the observed changes in morphology with redshift are physical rather than an artifact of bandpass shifting. A few examples are shown in Figure 3 (see color insert). Although interesting and occasionally dramatic morphological transformations are found between the WFPC2 and NICMOS images of some HDF galaxies, for the large majority of objects with peculiar or irregular WFPC2 morphologies, the peculiarities persist in the NICMOS images. The structure of dramatic "chain galaxies" like 2-736.1 ($z = 1.355$) in the HDF-N is almost entirely unchanging from 1300 Å to 6800 Å in the rest frame. Cowie et al (1995b) had noted that these peculiar structures were unlikely to be stable or persist for long, given the nominal dynamical timescales for these galaxies, and suggested that therefore they must be inherently young objects. For very blue galaxies like 2-736.1 this is likely to be true: The observed light from the UV through the IR is apparently dominated by the same relatively young generation of stars, and if there is an older stellar component distributed differently, then its visible light is swamped by the younger stars.

Although the more dramatic peculiarities in HDF galaxies generally persist from optical through IR wavelengths, there do nevertheless appear to be some general morphological trends with wavelength. Bulges and bars are found in NICMOS images of some $z \gtrsim 1$ disk galaxies that are invisible in the WPFC2 data, and disks appear to be smoother. From a preliminary analysis of structural parameters computed by Conselice et al (2000), we find that at $H_{160} \lesssim 24$, galaxies tend to have smaller half-light radii, to be more centrally concentrated, and to exhibit greater symmetry in the NICMOS images than in their WFPC2 counterparts. At fainter magnitudes, any trends are more difficult to discern because the mean galaxy size in the NICMOS data becomes small enough that the point-spread function (PSF)

dominates structural measurements. Teplitz et al (1998) noted similar trends in the distributions of structural parameters from NICMOS parallel images.

Abraham et al (1999a; 1999b) have studied a variety of other issues of galaxy morphology, concluding that the fraction of barred spirals declines significantly for $z > 0.5$; that ∼40% of HDF-N elliptical galaxies at $0.4 < z < 1$ have a dispersion of internal colors that implies recent, spatially localized star formation; that spiral bulges are older than disks; that the dust content of HDF spirals is similar to that locally; and that the peak of past star formation for a typical $z \sim 0.5$ spiral disk occurred at $z \sim 1$. These results are tentative because of small samples and uncertainties in stellar-population models, but they show promise for future deep surveys.

4.2 Galaxy Counts

One of the benefits derived from the ready availability of the reduced HDF data is that a variety of techniques have been used to catalog the sources (Williams et al 1996; Lanzetta er al 1996; Colley et al 1996; Sawicki et al 1997; Dell'Antonio & Tyson, 1996; Couch, 1996; Metcalfe et al 1996; Madau & Pozzetti, 1999; Chen et al 1999; Fontana et al 1999). Different algorithms have been used to construct the catalogs, but all at some level rely on smoothing the image and searching for objects above a surface brightness threshold set by the background noise. Ferguson (1998b) compared a few of the available catalogs and found reasonable agreement among them for sources brighter than $V_{606} = 28$, with systematic differences in magnitude scales of less than 0.3 (nevertheless, there *are* systematic differences at this level). The different catalogs apply different algorithms for splitting and merging objects with overlapping isophotes. These differences, together with the different schemes for assigning magnitudes to galaxies, result in overall differences in galaxy counts. At $I_{814} = 26$ the galaxy counts in the catalogs considered by Ferguson (1998b) all agree to within 25%, whereas at $I_{814} = 28$ there is a factor of 1.7 difference between them. This highlights the fact that galaxy counting is not a precise science.

Figure 4 shows the counts in four photometric bands derived from the HDF and from ground-based observations. As a fiducial comparison, a no-evolution model is shown for a spatially flat model with $\Omega_M = 0.3$ and $\Omega_\Lambda = 0.7$. In all bands the number–magnitude relation at HDF depths is significantly flatter than $N(m) \propto m^{0.4}$, but at blue wavelengths it exceeds the purely geometrical (no-evolution) predictions by roughly a factor of 3. Interpretation of the counts is addressed in more detail in Section 5.1.

4.3 Galaxy Sizes

One of the interesting and somewhat unexpected findings of HST faint-galaxy surveys has been the small angular diameters of faint galaxies. The sky is peppered with compact high-surface-brightness objects, in contrast to the expectation from $\Omega_M = \Omega_{tot} = 1$ pure-luminosity evolution (PLE) models (Section 5.1)

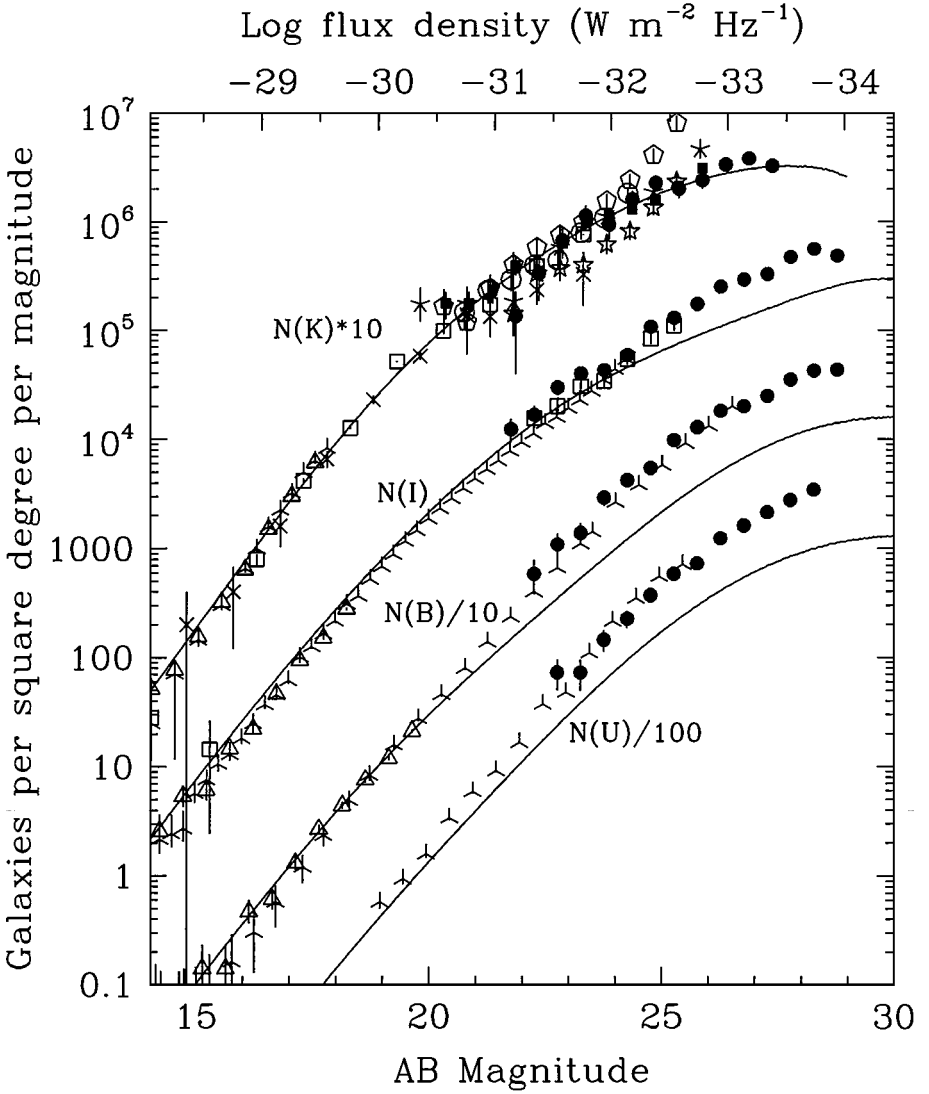

Figure 4 Galaxy counts from the HDF and other surveys. The HDF galaxy counts (solid symbols) use isophotal magnitudes and have not been corrected for incompleteness. These corrections will tend to steepen the counts at the faint end, but in a model-dependent way. For the *K*-band, a color correction of -0.4 mag has been applied to the NICMOS F160W band magnitudes. The HDF-N counts from Thomson et al (1999) are shown as filled squares while the HDF-S counts (Fruchter et al 2000) are filled circles. For the *U*, *B* and *I* bands, the HDF counts are the average of HDF-N (Williams et al 1996) and HDF-S (Casertano et al 2000) with no color corrections. The groundbased counts (open symbols) are from Mcleod & Rieke (1995), Gardner et al (1993; 1996), Postman et al (1998), Lilly Cowie & Gardner (1991), Huang et al (1997), Minezaki et al (1998), Bershady et al (1998), Moustakas et al (1997), and Djorgovski et al (1995). The smooth curves represent a no-evolution model with Ω_M, Ω_Λ, $\Omega_{\rm tot} = 0.3, 0.7, 0.1$ based on the luminosity functions, spectral-energy distributions, and morphological type mix of the "standard NE" model of Ferguson & McGaugh (1995).

and models dominated by low-surface-brightness (LSB) galaxies (Ferguson & McGaugh, 1995).

Galaxy radii can be measured using image moments (which are subject to severe biases because of isophotal thresholds), growth curves, or profile fitting. Ferguson (1998b) considered the size distribution derived from image moments, whereas Roche et al (1998) discuss the distribution of half-light radii derived from profile fitting. Roche et al (1998) find no evidence for evolution in the rest-frame sizes or surface brightnesses of normal spirals and ellipticals out to $z = 0.35$. At higher redshift they find evidence for strong evolution; galaxies are more compact and of higher surface brightness than expected from a PLE model (see also Schade et al 1995b). The sizes of disk galaxies were shown to be reasonably well matched by a size-luminosity evolution (SLE) model wherein spirals form stars gradually from the inside out. In a study with similar goals, Simard et al (1999) analyzed a sample of 190 (non-HDF) field galaxies with spectroscopic redshifts and HST images. They find no evidence for size or luminosity evolution of disk-dominated galaxies out to $z \sim 1$. The Simard et al (1999) analysis includes a more comprehensive treatment of selection biases and an empirical comparison to local samples that makes the results quite compelling. However, Simard et al (1999) do identify nine high-surface-brightness objects in their sample at $z > 0.9$. If these were included as disk galaxies, the results would be closer to those of Roche et al (1998). A comparison of the bivariate distribution of the Simard et al (1999) luminosities and scale lengths to a $z \sim 0$ sample suggests only moderate density evolution out to $z \sim 1.2$, with a decrease in the number density of bright, large-scale-size galaxies at higher redshift (de Jong & Lacey, 1999). Galaxies in the HDF with spectroscopic or photometric redshifts greater than $z = 2$ generally appear to be more compact than present-day L^* galaxies (Lowenthal et al 1997; Roche et al 1998).

At magnitudes fainter than $I = 25$, morphological classification and profile fitting become quite difficult because most galaxies at these faint magnitudes are so small that even with HST there are few independent resolution elements within the area detected above the background. Ferguson (1998b) studied the distribution of first-moment radii and modeled the selection boundaries of the HDF in size and magnitude. Because the first-moment radii are measured above a fixed isophote, the interpretation of the observed trends is highly model dependent, and is sensitive to the assumed redshift distribution and morphological-type distribution of the galaxies. Nevertheless, down to $I \sim 27$ the HDF counts are clearly dominated by galaxies more compact than local L^* spirals. At fainter magnitudes, the locus of HDF galaxy sizes is tightly constrained by selection, and there is very little information on the *intrinsic* size distribution of the objects.

4.4 Spectroscopic and Photometric Redshifts

The HDF-N and flanking fields have been the focus of some of the most intensive and complete spectroscopic redshift survey work on faint galaxies. Essentially all spectroscopic redshifts in the HDF have come from the W.M. Keck Observatory

and LRIS spectrograph (Cohen et al 1996, 2000; Lowenthal et al 1997; Phillips et al 1997; Steidel et al 1996, 1999; Dickinson, 1998; Adelberger et al 1998; Spinrad et al 1998; Weymann et al 1998; Waddington et al 1999; Zepf et al 1997; Hu et al 1998). The most recent compilation is 92% complete for $R < 24$ in the central HDF-N, and also 92% complete for $R < 23$ in the flanking fields (Cohen et al 2000). The median redshift is $z \approx 1$ at $R = 24$. Altogether, including unpublished redshifts from the Steidel group, more than 700 spectroscopic redshifts have been measured in the immediate vicinity of the HDF-N, with $\sim$150 in the central HDF (WF and PC) alone. This latter corresponds to 30 redshifts per arcmin^2, spanning $0.089 < z < 5.60$ (and a few stars), a density unmatched by any other field galaxy survey. At the same time, it is sobering to realize that less than 5% of the galaxies from the Williams et al (1996) HDF-N catalog have spectroscopic redshifts. The vast majority are fainter than the spectroscopic limit achievable with present-day telescopes. For the HDF-S, the extant spectroscopy is more limited, consisting of about 250 redshifts in an irregular area surrounding the three HST fields (Glazebrook et al 2000; Dennefeld et al 2000; Tresse et al 1999). Three galaxies at $2.8 < z < 3.5$ have been confirmed by the VLT (Cristiani 1999). Eleven HDF-S ISO sources have redshift measurements from VLT IR spectroscopy (Rigopoulou et al 2000).

The estimation of galaxy redshifts using broad-band colors received a tremendous boost from the HDF observations and followup studies. Indeed, the advent of the HDF marked a transition for photometric redshifts, which evolved from an experimental exercise to a widely used technique. This came about for several reasons. Perhaps foremost, as noted above, the WFPC2 HDF data readily detected galaxies as much as 100 times fainter than the practical spectroscopic limits of 10-m telescopes. Therefore, in order to interpret the properties of the vast majority of HDF galaxies, non-spectroscopic techniques for estimating redshifts are necessary. Fortunately, the HDF-N WFPC2 data set offered very-high-quality, four-band photometry from 0.3 to 0.8 μm for thousands of faint galaxies, and the extensive follow-up observations that came later extended this to other wavelengths and wider fields of view. Rapid dissemination of data and source catalogs from the HDF and follow-up observations made it relatively easy for any investigator to test their photometric redshift method. Indeed, it should be noted that many photometric redshift studies to date have been tested and calibrated *solely* using the HDF-N.

Several groups (Steidel et al 1996; Lowenthal et al 1997; Clements & Couch 1996; Madau et al 1996, 1998) used two-color selection keyed to the passage of the Lyman limit and Lyman α forest breaks through the F300W and F450W passbands to identify galaxy candidates at $z > 2$. Such color-selected objects are variously referred to as Lyman-break galaxies, or UV dropouts. The Madau et al (1996, 1998) studies were seminal in combining color-selected HDF samples at $z \sim 3$ and 4 with previous (spectroscopic, non-HDF) studies at $z < 2$ to derive a measure of the global history of cosmic star formation, a goal subsequently pursued by many other groups using various kinds of HDF photometric redshifts (see Section 5.5).

More general approaches to photometric redshifts have either fit redshifted spectral templates to the photometric data (e.g. Gwyn & Hartwick 1996; Mobasher et al 1996; Lanzetta et al 1996; Sawicki et al 1997; Fernandez-Soto et al 1999; Benítez et al 1999), or have used generalized polynomial fits of redshift vs. multi-band fluxes to a spectroscopic training set (e.g. Connolly et al 1997; Wang et al 1998). Cowie & Songaila (1996) and Connolly et al (1997) were the first to include IR HDF photometry when deriving photometric redshifts. In principle, this is especially useful in the $1 < z < 2$ range where it is difficult to measure redshifts from optical spectroscopy due to the absence of strong, accessible emission or absorption features, and where the strong spectral breaks (e.g. at 4000 Å and the 912 Å Lyman limit) fall outside the optical passbands. Many other groups have since included IR photometry in their photometric redshift work, using the KPNO 4-m *JHK* images from Dickinson et al (Fernandez-Soto et al 1999), or more recently HST NICMOS data (Thompson, 1999; Budavari et al 1999; Yahata et al 2000).

Hogg et al (1998) and Cohen et al (2000) have carried out blind tests of the accuracy and reliability of HDF photometric redshifts, comparing photometric predictions by the various groups with spectroscopic redshifts unknown to those groups when the predictions were made. In general, all of the photometric techniques are quite successful at $z \lesssim 1.4$, where the spectroscopic training sets are extensive, with the best prediction schemes achieving $|z_{\rm phot} - z_{\rm spec}|/(1 + z_{\rm spec}) \lesssim 0.05$ for $\gtrsim 90\%$ of the galaxies. At $z > 1.9$ the results are also generally quite good, with 10 to 15% RMS in $\Delta z/\ (1 + z)$ after excluding the worst outliers. The intermediate redshift range, where photometric redshifts are particularly interesting, has not yet been tested due to the lack of spectroscopic calibrators.

Photometric redshifts have been used to identify galaxy candidates in both HDFs at $z > 5$. Two objects noted by Lanzetta et al (1996) and Fernández-Soto et al (1999) have been subsequently confirmed by spectroscopy, with $z = 5.34$ and 5.60 (Spinrad et al 1998; Weymann et al 1998). With the addition of near–infrared data, it becomes possible, in principle, to push to still higher redshifts. Indeed, at $z > 6.5$, galaxies should have virtually no detectable optical flux. Candidates at these very large redshifts have been identified by Lanzetta et al (1998) and Yahata et al (2000). One of these in the HDF-N was readily detected in NICMOS 1.6 μm images by Dickinson et al (2000b), but is not significantly detected at J_{110} or at optical wavelengths. Although this is a plausible candidate for an object at $z \gtrsim 12$, there are also other possible interpretations. It is curious that several of the proposed $z > 10$ candidates, including this "*J*-dropout" object in the HDF-N and several of the HDF-S/NICMOS candidates proposed by Yahata et al (2000), are surprisingly bright ($\sim$1 μJy) at 2.2 μm. These would be significantly more luminous than the brightest known Lyman-break galaxies at $2 < z < 5$. It remains to be seen whether this points to some remarkable epoch of bright objects at $z > 10$, or whether instead the photometric redshifts for these objects have been overestimated.

4.5 Galaxy Kinematics

Spectroscopy of galaxies in the HDF-N has provided kinematical information leading to constraints on mass and/or luminosity evolution. Phillips et al (1997) and Guzman et al (1997) observed 61 compact, high-surface-brightness galaxies ($r < 0.''5$) in the HDF-N flanking fields. The great majority show emission lines and have redshifts $0.4 < z < 1$. Masses for the systems were deduced from the line widths, which ranged from 35–150 km s^{-1}, and one-half of the sample were found to be low mass ($M < 10^{10}\ M_{\odot}$), relatively luminous systems similar to local H II galaxies. The remaining systems were a heterogeneous class similar to local starburst galaxies.

Vogt et al (1997) studied a separate magnitude-limited sample of eight high-inclination disk galaxies from the HDF-N flanking fields in the redshift range $0.15 < z < 0.75$. Reliable velocity information could be discerned to three disk scale-lengths, comparable to the extent of optical rotation curves for local galaxies. Results from this survey were combined with an earlier survey of more luminous galaxies (Vogt et al 1996) to study the Tully-Fisher (TF) relation at $z \sim 0.5$ over a span of 3 magnitudes. A luminosity–line-width relation exists for the sample, linear and of the same slope as the local TF relation, but shifted to higher luminosities by 0.4 magnitudes. This is similar to the results from some other studies (Forbes et al 1996; Bershady, 1997) but larger amounts of luminosity evolution were seen in other samples (Rix et al 1997; Simard & Pritchet, 1998). Vogt et al (1997) speculate that the differences are due to sample selection. In any case, the modest luminosity evolution is consistent with the modest surface-brightness evolution found in the analysis of structural parameters by Simard et al (1999).

4.6 Mid-IR Sources

Mid-IR observations offer the opportunity to detect emission from material heated by star formation or active galactic nuclear (AGN) activity and thus provide some indication of radiative activity that may be obscured at UV through near-IR wavelengths. The launch of the *Infrared Space Observatory* (ISO), the first space-based mid-IR telescope capable of such observations, coincided nicely with the availability of the HDF data set, and both deep fields (N and S) were the targets of deep 6.75 μm and 15 μm observations with the ISOCAM imager. The HDF-S ISO observations were made before the HST imaging was carried out, and they are currently being analyzed (e.g Oliver et al 2000).

The HDF-N ISO observations were carried out using discretionary time allocated by the ISO director to an observing team led by Rowan-Robinson (Serjeant et al 1997; Goldschmidt et al 1997; Oliver et al 1997; Mann et al 1997; Rowan-Robinson et al 1997). Two other groups have subsequently processed and reanalyzed the ISO data using independent methods (Désert et al 1999; Aussel et al 1999a). The 15 μm maps extend well beyond the central HDF to cover a portion

of the flanking fields, and have $\approx 9''$ resolution. The high-sensitivity region of the 6.7 μm maps is smaller and roughly matched to the central HDF WFPC2 area, with $\approx 4''$ resolution.

The depth of the ISO image mosaics varies over the field of view, and the data processing procedures are complex and the subject of continuing refinement. Extensive simulations have been used by the three groups to calibrate source detection, completeness and reliability, and photometry. Given these complexities, it is perhaps not unexpected that the groups have produced different source catalogs. A simple, visual inspection of the images presented by Serjeant et al (1997) or Aussel et al (1999a) demonstrates that the 15 μm data is much more straightforward to interpret—at least $\sim$20 sources are readily visible to the eye, whereas the 6.7 μm image has only a few "obvious" sources and much more low-level background structure. Indeed, the source catalogs from the three groups agree reasonably well at 15 μm, commonly detecting most of the brighter sources ($\sim$20 detections with $\gtrsim$200 μJy) with generally similar measured flux densities. Aussel et al (1999a) and Désert et al (1999), however, claim reliable source detection to fainter flux limits than do Goldschmidt et al (1997) and thus have longer source lists: The complete plus supplemental catalog of Aussel et al lists 93 sources at 15 μm. At 6.75 μm, the situation is more confused (perhaps literally). All three groups define "complete" lists of six or seven sources, but they are not all the same objects. Differences in the assumptions about ISO astrometry and geometric distortion corrections may be partially responsible. Goldschmidt et al provide a list of 20 supplemental sources at 6.7 μm, only a few of which are detected by the other groups. There also appear to be systematic differences in the derived source fluxes at this wavelength. Altogether, the 15 μm source detections and fluxes appear to be well established, but only the few brightest 6.7-μm detections are unambiguous, and the associated fluxes may be uncertain.

The optical counterparts of the HDF-N ISO sources are mostly brighter galaxies at $0 < z < 1.2$, although occasionally the identifications may be confused because of the $9''$ PSF at 15 μm. Many of the 15 μm sources also correspond to radio sources (few or none, however, correspond to the SCUBA sources discussed below). Over this redshift range, the 15 μm measurements primarily sample emission from the "unidentified emission bands," including the strong features at 6.2–8.6 μm. These features are considered a characteristic signature of star-forming galaxies (see, e.g. Rigopoulou et al 1999). At $z > 1.4$, they shift out of the 15 μm ISO bandpass, and therefore more distant objects should become much fainter. Indeed none have been identified yet in the ISO/HDF. Warm dust ($T > 150$ K) may also contribute to the mid-IR emission, and some of the ISO sources are almost certainly AGN (e.g. HDF 2-251, a red early-type radio galaxy at $z = 0.960$, whose mid-IR emission is very likely not powered by star formation). Most of the HDF/ISO galaxies do not appear to be AGN, however, and if powered by reprocessed stellar UV radiation have obscured star formation rates that greatly exceed those derived from their UV/optical emission (Rowan-Robinson et al 1997). Assuming an M82-like

spectrum to derive *k*-corrections, the average HDF/ISO source is roughly $10\times$ more luminous than M82 at 15 μm (Elbaz et al 1999). Rowan-Robinson (1999) estimates that roughly two thirds of the star-formation at $z \sim 0.5$ is in dust-enshrouded starbursts such as those detected by ISO.

4.7 Sub-Millimeter Sources

The commissioning of the sub-millimeter bolometer array camera SCUBA on the JCMT has opened a potentially revolutionary new window on the distant universe, permitting the detection of dust-reradiated energy from starburst galaxies and AGN out to almost arbitrarily large redshifts (thanks to the strongly negative *k*-correction at 850 μm, where SCUBA is most sensitive). A series of SCUBA surveys (e.g. Smail et al 1997; Barger et al 1998) have now resolved a source population that comprises a substantial fraction of the far-IR background measured by COBE and that may account for a significant fraction of the global radiative energy density from galaxies. One of the first and deepest of such surveys was carried out by Hughes et al (1998), who observed the HDF for 50 hours, detecting five sources at 850 μm to a 4.4σ limit of 2 mJy. Given the $15''$ SCUBA beam size and possible pointing uncertainties, the optical identifications for many (if not all) of these five sources remain in doubt, and some may be blends due to multiple objects. The brightest source, however, was subsequently pinpointed by a 1.3 mm interferometric observation from Institute de Radioastronomie Millimetrique (IRAM) (Downes et al 1999). Unfortunately, this accurate position (which coincides with a microjansky radio source) did not fully settle the identification of the optical counterpart, falling halfway between two HDF galaxies separated by $2''$ (and almost certainly at very different redshifts). The second brightest SCUBA source, falling just outside the primary WFPC2 field, has no obvious counterpart in the flanking field WFPC2 images, nor in the NICMOS data of Dickinson et al (2000b).

Taking advantage of the frequent (but not universal) association of sub-millimeter sources with centimeter radio detections, Barger et al (1999) have used SCUBA to observe 14 radio sources in the HDF flanking fields with optical and near-IR counterparts fainter than $I > 25$ and $K > 21$, respectively. They surveyed roughly half of the flanking field area to a 3σ depth of 6 mJy, detecting five of the "blank field" radio source targets in addition to two new radio-quiet sub-millimeter sources; however, none of the optical/near-IR bright sources were detected at 850 μm. For those sub-millimeter sources with radio counterparts, photometric redshifts from the 850 μm to 20 cm flux ratio (Carilli & Yun, 1999; Barger et al 1999; Cowie & Barger, 1999) suggest that most lie in the redshift range $1 < z < 3$. Sub-millimeter sources without radio counterparts may represent a higher redshift tail.

The HDF-N has also been imaged at 450 μm (Hughes et al 1998) and 2.8 mm (Wilner & Wright, 1997). No sources were detected at either wavelength, which is not surprising given the flux densities of the 850 μm detections.

4.8 Radio Sources

The HDF-N has become one of the best-studied regions of the sky at radio wavelengths, and the availability of extremely deep optical/IR imaging and extensive spectroscopy has made it arguably the most important survey for understanding the properties of "average" radio sources at the millijansky and microjansky level. The VLA and MERLIN arrays have been used to map regions including the HDF-N at 3.5 cm and 20 cm wavelengths (Fomalont et al 1997; Richards et al 1998, 1999; Muxlow et al 1999; Richards, 2000). The combined MERLIN + VLA data have been used to make high-resolution maps of 91 HDF radio sources, permitting a detailed study of radio source extent, as well as pinpointing locations for a few ambiguous identifications and confirming the blank field character of others. Altogether, 16 radio sources are located in the central HDF-N WFPC2 field, and many more in the flanking fields.

The optical counterparts for most of the radio sources (72 of 92 in the region with suitably deep imaging) are relatively bright galaxies ($\langle I \rangle \approx 22$) at $0.4 < z < 1$. Apart from a few manifestly AGN-powered objects, usually giant elliptical radio galaxies (including the $z = 1.02$ galaxy HDF 4-752.1), most are disk galaxies, sometimes disturbed or interacting. For nearly all, the radio emission is resolved with a typical size $\sim 1''$, reinforcing the evidence that it primarily arises from star formation. However, about 20% of the sources have very faint or optically invisible counterparts with $I \gtrsim 25$. Many of these have *K*-band identifications with very red optical-IR colors (Richards et al 1999). Waddington et al (1999) have studied one red HDF radio source which is apparently at $z = 4.4$ (from a single-line spectroscopic redshift). Several have been detected in 850 μm observations with SCUBA (Barger et al 1999). These "invisible" radio sources appear to be a population discontinuous from the majority of the optically brighter sources, and may be high-redshift, dust-obscured, vigorously star-forming systems. Finally, two VLA sources in the HDF proper have no optical counterparts to the limits of the WFPC2 data, and one (123646+621226) has no counterpart to the extremely faint limit of the NICMOS GTO HDF field.

The HDF-S was observed by the Australia Telescope National Facility (ATNF) in 1998. The first year's observations covered a $60'$ diameter region at 20 cm detecting 240 sources down to 100 μJy (13 in the primary WFPC2 field) and correspondingly smaller fields at 13, 6, and 3 cm. These have now been augmented by substantially deeper observations which are currently being analyzed (Norris et al 2000), but which should reach 5σ sensitivities of 40 μJy at 13 and 6 cm.

4.9 Active Galactic Nuclei

The number-density of AGN at HDF depths is of great interest because of its connection to the X-ray background and to the re-ionization of the universe at high redshift. Jarvis & MacAlpine (1998) identified 12 possible candidates with colors and morphologies consistent with AGN at $z > 3.5$. A similar study by Conti

et al (1999) found no candidates above $z = 3.5$ and an upper limit of 20 candidates at lower z. These relatively low number densities support the prevailing view that the UV emission from AGN at high redshifts is insufficient to account for the ionization of the IGM, and they also suggest that black holes do not form with constant efficiency within cold-dark-matter halos (Haiman et al 1999). Fainter AGN yet to be identified may lie within the HDF. Based on the properties of many of the optical counterparts to faint ROSAT X-ray sources, Almaini & Fabian (1997) estimate that roughly 10% of the galaxies in the HDF are likely to be X-ray luminous, narrow-lined AGN. However, few of the optically identified AGN candidates in the HDF-N are detected in the X-rays by the Chandra observatory (Hornschemeier et al 2000).

4.10 Gravitational Lensing

The depths of the HDFs have made them well suited for studies of gravitational lensing. As Blandford (1998) noted in his review, based on a rule of thumb from the number of lensed quasars and radio sources in other surveys, roughly 0.2% of the galaxies, corresponding to five to ten sources, were expected to be strongly lensed (producing multiple images) in each HDF field. In addition, weak lensing by large-scale structure and individual galaxies should slightly distort most of the galaxy images. Initial visual inspection of the HDFs produced a number of possible strong lensing candidates (Hogg et al 1996; Barkana et al 1999), but none has yet been confirmed by spectroscopy. Rather, a few of the brighter examples appear not to be lensed systems, but only chance superpositions (Zepf et al 1997). A few candidates remain in each of the primary WFPC2 HDF fields (Barkana et al 1999), but it will require spectroscopy of very faint sources to confirm their nature.

An analysis of the HDF-N images by Zepf et al (1997) concluded that there were at most one to two strongly lensed sources in the entire field, although very faint objects with small angular separation could have escaped detection. On this basis they suggested that the HDF data were not compatible with a large cosmological constant. Cooray et al (1999) took this further by utilizing published photometric redshifts for the galaxies in the HDF-N to calculate the expected number of multiply-imaged galaxies in the field. They found that a limit of one detectable strongly lensed source requires $\Omega_\Lambda - \Omega_M < 0.5$. For Ω_M, Ω_λ, $\Omega_{\rm tot} =$ 0.3, 0.7, 1, they predict 2.7 multiply-imaged galaxies. The lensing statistics are thus, in spite of earlier expectations for a larger number of lenses, not in conflict with recent determinations of Ω_Λ from high-redshift SN (Perlmutter et al 1999; Riess et al 1998).

Weak lensing is manifested by a tangential shear in the image of the more distant source, and the amount of ellipticity, or polarization p, introduced by a typical closely-spaced galaxy pair is of the order of $p \sim 10^{-2}$. It is possible to attempt a statistical detection by looking for the effect superimposed on the intrinsic morphologies of the source galaxies perpendicular to galaxy-galaxy lines

of sight. As a differential effect, weak-lensing distortion is far less sensitive to the cosmological model than to the masses or surface densities of the intervening deflector galaxies. Using color and brightness as redshift indicators, Dell' Antonio & Tyson (1996) defined a sample of 650 faint background and 110 lens galaxies in the HDF-N and reported a 3σ detection equivalent to $p = 0.06$ for galaxy-lens pairs having a separation of $2''$. This corresponds to an average galaxy mass of $6 \times 10^{11}\ M_{\odot}$ inside 20 kpc, or an internal velocity dispersion of 185 km s^{-1}. A similar analysis of HDF-N images was subsequently performed by Hudson et al (1998), who used photometric redshifts to determine distances of lens and source galaxies, and who discriminated between lensing galaxy types based on colors. Limiting their analysis to separations greater than $3''$, they succeeded in measuring background shear at a 99% confidence level, finding that intermediate-redshift spiral galaxies follow the Tully-Fisher relation but are 1 mag fainter than local spirals at fixed circular velocity. Although the sense of the evolution is the opposite of that found in the kinematical studies, given the uncertainties, the lensing result is consistent with the modest luminosity-evolution observed by Vogt et al (1997) when the studies are compared using the same cosmology. The lensing results are inconsistent with the larger luminosity evolution found by Rix et al (1997) and Simard & Pritchet (1998).

4.11 Intergalactic Medium

The HDF-S STIS field was selected to contain the bright, moderate redshift quasar J2233-606. Deep HST imaging of the field around the quasar during the HDF-S campaign has provided detection and morphologies of numerous galaxies near the line of sight. Moderate- to high-resolution spectra have been obtained of the quasar both from the ground and with HST covering the wavelength regime 1140-8200 Å (Savaglio, 1998; Sealey et al 1998; Outram et al 1999; Ferguson et al 2000), whereas follow-up observations from the ground have established the redshifts of some of the brighter galaxies in the field (Tresse et al 1999). Too few redshifts have yet been measured to allow detailed study of the correspondence between galaxies and QSO absorbers. A tentative detection of Lyα emission surrounding the QSO was reported by Bergeron et al (1999).

Using the STIS UV and ground-based optical spectra, Savaglio et al (1999) found the number density of Lyα clouds with $\log N_{\rm HI} > 14$ in the redshift interval $1.5 < z < 1.9$, to be higher than that found in most previous studies, and saw no evidence for a change in the Doppler parameters of the Lyα lines with redshift. The two-point correlation function of Lyα clouds shows clear clustering on scales less than 300 km s^{-1}, especially the higher column density systems, in agreement with results from other quasars. Metal abundances in several absorption line systems have been studied by Prochaska & Burles (1999). Petitjean & Srianand (1999) studied the metal lines in the absorption-line systems near the QSO redshift and found that relative line strengths of different species are best modeled with a multi-zone partial-covering model wherein different species (e.g. Ne VIII, O

VI) arise from gas at different distances from the AGN, and the clouds cover the central continuum emission region completely but only a fraction of the broad emission-line region.

4.12 Galaxy Clustering

The measurements of clustering using the HDF have varied in the catalog and object selection, in the angular scales considered, in the use or non-use of photometric redshifts, and in the attention to object masking and sensitivity variations. In an early paper on the HDF-N, Colly et al (1996) explored whether the galaxy counts in the HDF are "whole numbers," i.e. whether fragments of galaxies were incorrectly being counted as individual galaxies. From an analysis of the angular correlation function of objects with color-redshifts $z > 2.4$ they conclude that many of these objects are HII regions within a larger underlying galaxy. This analysis showed a strong clustering signal on scales $0''.2 < \theta < 10''$. Colley et al (1997) explored various hypotheses for the neighboring galaxies and favored a scenario in which the faint compact sources in the HDF are giant star-forming regions within small Magellanic irregulars.

It is not clear whether the Colley et al (1996, 1997) results apply to other catalogs, given the different cataloging algorithms used. In particular, programs such as SExtractor (Bertin & Arnouts, 1996) and FOCAS (Tyson & Jarvis, 1979) use sophisticated and (fortunately or unfortunately) highly tunable algorithms for merging or splitting objects within a hierarchy of isophotal thresholds. The DAOFIND algorithm used by Colley et al (1996) provides no such post-detection processing. The extent to which this affects the results can only be determined by an object-by-object comparison of the catalogs, which has not (yet) been done in any detail. Ferguson (1998b) (Figures 1–4) presents a qualitative comparison of several catalogs (not including that of Colley et al) which shows significant differences in how objects with overlapping isophotes are counted. The Colley et al (1997) analysis focused specifically on 695 galaxies with color-redshifts $z > 2.4$. This number of galaxies is considerably larger than the 69 identified by Madau et al (1996), using very conservative color selection criteria, or the 187 identified by Dickinson (1998) with somewhat less conservative criteria. For these smaller samples, we suspect that the "overcounting" problem is not as severe as Colley et al contend.

Problems separating overlapping objects, although important for clustering studies on small angular scales, do not have much effect on the overall galaxy number–magnitude relation (Ferguson, 1998b) or angular clustering measurements on scales larger than $\sim 2''$.

Other studies of clustering in the HDF have been restricted to separations larger than $2''$. The analysis has focused primarily on the angular correlation function $\omega(\theta)$, which gives the excess probability δP, with respect to a random Poisson distribution of n sources, of finding two sources in solid angles $\delta\Omega_1$, $\delta\Omega_2$ separated by angle θ:

$$\delta P = n^2 \delta\Omega_1 \delta\Omega_2 \, [1 + \omega(\theta)]. \quad (1)$$

The angular correlation function is normally modeled as a power law

$$\omega(\theta) = A(\theta_0)\theta^{1-\gamma}. \quad (2)$$

Because of the small angular size of the field, $\omega(\theta)$ is suppressed if the integral of the correlation function over the survey area is forced to be zero. Most authors account for this "integral constraint" by including another parameter and fitting for $\omega(\theta) = \mathrm{A}(\theta_0)\theta^{1-\gamma} - C$, with a fixed value of $\gamma = 1.8$ and with A and C as free parameters.

Villumsen et al (1997) measured the overall angular correlation function for galaxies brighter than $R = 29$ and found an amplitude $A(\theta = 1'')$ decreasing with increasing apparent magnitude, roughly consistent with the extrapolation of previous ground-based results. The measured amplitude was roughly the same for the full sample and for a subsample of red galaxies (considered typically to be at higher redshift). The motivation for this color cut was to try to isolate the effects of magnification bias due to weak lensing by cosmological large-scale structure (Moessner et al 1998), but the predicted effect is small and could not be detected in the HDF (and will ultimately be difficult to disentangle from the evolutionary effects discussed in Section 5.6)

The remaining HDF studies have explicitly used photometric redshifts. Connolly et al (1999) considered scales $3'' < \theta < 220''$ and galaxies brighter than $I_{814} = 27$. Within intervals $\Delta z = 0.4$ the amplitude $\mathrm{A}(\theta = 10'') \sim 0.13$ shows little sign of evolution out to $z_{\mathrm{phot}} = 1.6$ (the highest considered by Connolly et al). Roukema et al (1999) analyzed a U-band selected sample, isolated to lie within the range $1.5 < z_{\mathrm{phot}} < 2.5$ and angular separations $2'' < \theta < 40''$. The results are consistent with those of Connolly et al (1999), although Roukema et al (1999) point out that galaxy masking and treatment of the integral constraint can have a non-negligible effect on the result.

Measurements of $\omega(\theta)$ for samples extending out to $z_{\mathrm{phot}} > 4$ have been carried out by Magliocchetti & Maddox (1999), Arnouts et al (1999) and Miralles & Pello (1998). The minimum angular separations considered for the three studies were $9''$, $5''$, and $10''$, respectively: i.e. basically disjoint from the angular scales considered by Colley et al (1997). All three studies detect increased clustering at $z \gtrsim 2$, although direct comparison is difficult because of the different redshift binnings. The interpretation shared by all three studies is that the HDF shows strong clustering for galaxies with $z \gtrsim 3$, in qualitative agreement with Lyman-break galaxy studies from ground-based samples (Giavalisco et al 1998; Adelberger et al 1998). Although this may be the correct interpretation, the significant differences in the photometric redshift distributions and the derived clustering parameters from the three studies leave a considerable uncertainty about the exact value of the clustering amplitude. The two most comprehensive studies differ by more than a factor of 3 in $A(\theta = 10'')$ at $z = 3$ (Arnouts et al 1999; Magliocchetti & Maddox, 1999). Both studies use photometric redshifts to magnitudes $I_{814} = 28$, which is fainter than the detection limits in the F300W and F450W bands for even flat-spectrum galaxies. A large part of the disagreement may thus be due to

scatter in $z_{\rm phot}$. The analysis also hinges critically on the assumed power-law index $\gamma = 1.8$ and the necessity to fit the integral constraint. Thus, although it seems reasonably secure that a positive clustering signal has been measured in the HDF at high $z_{\rm phot}$, it will require much larger data sets to constrain the exact nature of this clustering and determine its relation to clustering at lower redshift.

At brighter magnitudes, spectroscopic surveys show clear evidence for clustering in redshift space (Cohen et al 1996; Adelberger et al 1998; Cohen, 1999), with pronounced peaks even at redshifts $z > 1$. These structures, and others within the flanking fields, do not show evidence for centrally concentrated structures, and are probably analagous to walls and filaments observed locally.

5. INTERPRETATION

5.1 Galaxy Counts vs. Simple Models

The time-honored method of comparing cosmological models to field-galaxy surveys has been through the classical number–magnitude, size–magnitude, magnitude–redshift, etc. relations (Sandage, 1988). Much of this effort, including early results from the HDF, has been reviewed in Ellis (1997). There are three important changes to the scientific landscape that we must acknowledge before proceeding to discuss the more recent interpretation of the HDF number counts. The first change is the transition (motivated by high-z SNe Ia, cluster baryon fractions, etc.) from a favored cosmology with $\Omega_M = \Omega_{\rm tot} = 1$ to one with Ω_M, Ω_Λ, $\Omega_{\rm tot} = 0.3, 0.7, 1$. The latter cosmology comes closer to matching the galaxy counts without extreme amounts of evolution. The second change is the realization that galaxy counts at HDF depths push to depths where the *details* of galaxy formation become extremely important. Models that posit a single "epoch of galaxy formation" were never realistic, and are no longer very useful. Finally, it has become more popular to model quantities such as the metal enrichment history $\dot{\rho}_z(z)$ than it is to model galaxy counts. Consequently, to our knowledge there are no published papers that compare the overall $N(m)$ predictions of hierarchical semi-analytic models with the currently favored cosmology to the HDF galaxy counts.

5.1.1 No-Evolution (NE) Models The assumption of no evolution is not physically reasonable, but provides a useful fiducial for identifying how much and what kinds of evolution are required to match faint-galaxy data. Traditional no-evolution models are based on estimates of the $z = 0$ luminosity functions for different types of galaxies. Bouwens et al (1997) construct a non-evolving model from the HDF itself, using 32 galaxies brighter than $I_{814} = 22.3$ to define a fiducial sample. They construct Monte-Carlo realizations of the HDF that might be seen from a universe uniformly populated with such galaxies, shifted to different redshifts and k-corrected on a pixel-by-pixel basis. This kind of simulation

automatically incorporates the selection and measurement biases of the HDF at faint magnitudes. It also normalizes the model *by fiat* to match the counts at $I_{814} = 22.3$, where traditional no-evolution models, normalized to the local luminosity function, already see significant discrepancies for the Einstein–de Sitter model. The resulting models underpredict the HDF counts at $I_{814} = 27$ by factors of 4 and 7 for models with $\Omega_M = 0.1$ and 1.0 (with $\Omega_\Lambda = 0$), respectively. The angular sizes of galaxies in the models are also too big at faint magnitudes, with a median half-light radius about a factor of 1.5 larger than that observed for galaxies with $24 < I < 27.5$. Because the typical redshift of the template galaxies in this model is $z \sim 0.5$, this model comparison suggests that much of the evolution in galaxy number densities, sizes, and luminosities occurs at higher redshift. The typical small sizes of faint galaxies essentially rule out low-surface-brightness galaxies (Ferguson & McGaugh, 1995; McLeod & Rieke, 1995) as a significant contributor to the counts at magnitudes $I_{814} > 20$ (Ferguson, 1999).

5.1.2 Pure Luminosity Evolution Models Many of the models that have been compared to the HDF number counts are variants of *pure luminosity evolution* (PLE) models (Tinsley, 1978), wherein galaxies form at some redshift z_f, perhaps varying by type, with some star-formation history $\psi(t)$. There is no merging. Metcalfe et al (1996) compare several different models to the counts and colors of galaxies in the HDF and in deep images taken at the William Herschel Telescope. For low Ω a reasonable fit to $I \approx 26$ is achieved, but the model progressively underpredicts the counts to fainter magnitudes, and the long star-formation timescales and heavily dwarf-dominated IMF adopted for ellipticals in this model seem inconsistent with the fossil evidence in local ellipticals. By including a simple prescription for dust attenuation, Campos & Shanks (1997) are able to achieve a reasonable fit to the counts for low Ω_M without resorting to a peculiar IMF. Another set of PLE models was considered by Pozzetti et al (1998), with emphasis on the near-UV counts and the effect of UV attenuation by intergalactic neutral hydrogen. From color-magnitude relations and a study of the fluctuations in the counts in the different HDF bands, Pozzetti et al (1998) conclude that at $B_{450} = 27$ roughly 30% of the sources in the HDF are at $z > 2$. The PLE model considered has $\Omega_M = 0.1$ with no cosmological constant, and with a redshift of formation $z_f = 6.3$. This model matches the counts quite well but predicts that about 80 objects brighter than $V_{606} = 28$ should disappear from the F450W band because of their high redshift, although Madau et al (1996) identify only about 15 such sources. Ferguson & Babul (1998) considered another low–Ω PLE model and encountered similar problems, predicting roughly 400 B-band Lyman-break objects, where only 15 or so were observed. The utility of PLE models clearly breaks down for $z \gtrsim 2$, where the details of galaxy formation become critical.

5.1.3 Models with Additional Galaxy Populations The great difficulty in achieving a fit with $\Omega_M = \Omega_{\rm tot} = 1$, even to ground-based galaxy counts, motivated investigations into different kinds of galaxies that might be missed from the census

of the local universe but could contribute to the counts of galaxies at faint magnitudes (Ferguson & McGaugh, 1995; Babul & Ferguson, 1996; Koo et al 1993; McLeod & Rieke, 1995). Perhaps the most physically motivated of these more exotic possibilities is the idea that the formation of stars in low-mass galaxy halos could be inhibited until low redshifts $z \gtrsim 1$ because of photoionization by the metagalactic UV radiation field (Efstathiou, 1992; Babul & Rees, 1992). Ferguson & Babul (1998) compared the predictions of such an $\Omega_M = 1$ "disappearing dwarf" model in detail to the HDF. They found that the simplest version of the model (*a*) overpredicts the counts at faint magnitudes, and (*b*) overpredicts the sizes of very faint galaxies. These problems are caused by the fact that, for a Salpeter IMF, the dwarfs fade too slowly and would still be visible in great numbers in the HDF at redshifts $z < 0.5$. Campos (1997) considered a model with much milder evolution, with each dwarf undergoing a series of relatively long (a few $\times\ 10^8$ yr) star-formation episodes. Acceptable fits to the counts and colors of galaxies are achieved both for high and low values of Ω. Both the Ferguson & Babul (1998) and the Campos (1997) models predict that the HDF sample at $I > 25$ is dominated by galaxies with $z < 1$, a result inconsistent with existing photometric-redshift measurements. Using a volume-limited photometric redshift sample to construct the bivariate brightness distribution of galaxies with $0.3 < z < 0.5$, Driver (1999) concludes that the volume density of low-luminosity, low-surface-brightness galaxies is not sufficient to explain the faint-blue excess either by themselves or as faded remnants. Further constraints on the low-redshift, low-luminosity population can be expected from the HDF STIS UV observations.

5.2 The Morphology of High-Redshift Galaxies

As was described in Section 4.1, HST images from the HDF and other surveys have established that the fraction of irregular and peculiar galaxies increases toward faint magnitudes (down to $I \sim 25$, where galaxies become too small for reliable classification). Some of the morphological peculiarities in HDF galaxies may be the consequence of interactions, collisions, or mergers. A higher merger rate at earlier epochs is a natural consequence of models that assemble the present-day Hubble sequence galaxies by a process of hierarchical mergers (Baugh et al 1996). In the local universe, morphological asymmetry correlates reasonably well with color, with late type, blue galaxies and interacting objects showing the greatest asymmetry (Conselice et al 1999). In the HDF, however, there are also highly asymmetric galaxies with *red* rest-frame $B - V$ colors as well as blue ones, and the asymmetries persist at NICMOS wavelengths (cf. Figure 9), where longer-lived stars in a mixed-age stellar population would dominate the light and where the obscuring effects of dust would be reduced. The timescale over which an interacting galaxy will relax and regularize should be shorter ($\gtrsim$1 Gyr) than the time over which stars formed during the interaction would burn off the main sequence, and thus if star formation occurs during collisions then blue colors should persist longer than the most extreme manifestations of morphological disturbance.

Conselice et al (2000) suggest that the large number of asymmetric HDF galaxies demonstrates the prevalence of early interactions and mergers, some of which (the bluest objects) have experienced substantial star formation during the encounter, whereas others have not (or, alternatively, have their recent star formation obscured by dust).

Although interactions seem an attractive way of explaining these morphological peculiarities, it is nevertheless worth mentioning some qualifications concerning the details of the models which have been tested to date. First, although a high merger rate at relatively low redshifts is a generic prediction of the standard cold dark matter (SCDM) model, models with lower Ω_M have a substantially lower merger rate at $z < 1$. The Baugh et al (1996) model that was explicitly compared with the HDF was based on the SCDM cosmology. Second, even with the high merger rate the Baugh et al (1996) model predicts that galaxies that have had major merger within 1 Gyr prior to the time of observation constitute less than 10% of the total population at $I = 25$ (their Figure 2). Most of the irregular galaxies in this model are simply bulgeless, late-type galaxies. Im et al (1999) have studied the redshift distribution of galaxies with $17 < I < 21.5$ and conclude that the irregular/peculiar class is a mix of low-redshift dwarf galaxies and higher-redshift ($0.4 < z < 1$) more luminous galaxies. These higher redshift galaxies are unlikely to be the progenitors of present-day dwarf irregular galaxies, but it is not clear whether they are predominantly low-mass galaxies undergoing a starburst, or more massive galaxies undergoing mergers. The scatter in colors and sizes suggests it is a mix of both, but more detailed kinematical information is needed.

5.3 Elliptical Galaxies

The simple picture of the passively evolving elliptical galaxy, formed at high redshift in a single rapid collapse and starburst, has held sway since the scenario was postulated by Eggen et al (1962) and its photometric consequences were modeled by Larson (1974) and Tinsley & Gunn (1976). This hypothesis is supported by the broad homogeneity of giant elliptical (gE) galaxy photometric and structural properties in the nearby universe, and by the relatively tight correlations between elliptical galaxy chemical abundances and mass or luminosity. Observations in the past decade have pushed toward ever higher redshifts, offering the opportunity to directly watch the evolutionary history of elliptical galaxies. Most of this work has concentrated on rich cluster environments, and is not reviewed here except to note that most observers have favored the broad interpretation of quiescent, nearly passive evolution among cluster ellipticals out to $z \approx 1$ (e.g. Aragón-Salamanca et al 1993; Stanford et al 1995, 1998; Ellis et al 1997; van Dokkum et al 1998; De Propris et al 1999).

The "monolithic" formation scenario serves as a rare example of a clearly stated hypothesis for galaxy evolution against which to compare detailed measurements and computations. The alternative "hierarchical" hypothesis is that elliptical galaxies formed mostly via mergers of comparable-mass galaxies that had at the time

of merging already converted at least some of their gas into stars (e.g. Kauffmann et al 1993). The argument between the monolithic and the hierarchical camps is not about the origin of galaxies from gravitational instability within a hierarchy of structure, but rather about when gEs assemble most of their mass and whether they form their stars mostly *in situ* or in smaller galaxies that subsequently merge. At least one observational distinction is clear: In the hierarchical model the number density of elliptical galaxies should decrease with redshift. In the monolithic model the number density should remain constant and the bolometric luminosities should increase out to the epoch of formation.

Measuring the density and luminosity evolution of the *field* elliptical population, however, has proven difficult, and many different approaches, perhaps complementary but not necessarily concordant, have been used to define suitable galaxy samples. Recent debate has focused on estimates of the evolution of the co-moving density of passively-evolving elliptical galaxies in the Canada-France Redshift Survey (Lilly et al 1995b). Applying different photometric selection criteria and different statistical tests, two groups (Lilly et al 1995a; Totani & Yoshii, 1998) found no evidence for density evolution out to $z = 0.8$, whereas another group (Kauffmann et al 1996), found evidence for substantial evolution. This debate highlights the difficulties inherent to defining samples based on a color cut in the margins of a distribution, where small changes in the boundary, as well as systematic and even random photometric errors in the data, can have substantial consequences for the conclusions.

HST makes it possible to define samples of distant galaxies morphologically. The multicolor HDF images provide an attractive place to study distant ellipticals, but because of its very small volume and the inherently strong clustering of elliptical galaxies, one must be careful in drawing sweeping conclusions from HDF data alone. Thus, although we focus our attention primarily on the HDF results, they should be considered in context with results from other surveys (e.g. Driver et al 1995; Glazebrook et al 1995; Driver et al 1998; Treu et al 1999; Treu & Stiavelli 1999).

The interpretation of the high-redshift elliptical galaxy counts depends in large measure on a comparison to the *local* luminosity function (LF) of elliptical galaxies. The basic parameters of published LFs for local elliptical galaxies (or what are sometimes assumed to be elliptical galaxies)[3] span a very wide range in normalization, characteristic luminosity, and faint end behavior. Early HST studies such as that by Im et al (1996) concluded that NE or PLE models were consistent with elliptical-galaxy number counts predicted using the local LF of Marzke et al (1994).

Searches for distant elliptical galaxies in the HDFs have relied on either color or morphology. In the HDF-N, Fasano et al (1998) and Fasano & Filippi (1998), along with Schade et al (1999) for the CFRS and LDSS surveys, all examined the

[3]Even locally, classification uncertainties may be partly responsible for the widely diverse measurements of the elliptical galaxy LF (see Loveday et al 1992; Marzke et al 1994, 1998; Zucca et al 1994; Sandage 2000).

size-luminosity relation for morphologically-selected ellipticals, finding evolution out to $z \sim 1$ consistent with PLE models. Kodama et al (1999) found a well-defined color-magnitude sequence at $\langle z \rangle \sim 0.9$, consistent with passive evolution for approximately half the galaxies, but they also noted a substantial "tail" of bluer objects. Similarly, in the Schade et al (1999) study, about one third of the sample at $z > 0.5$ had [OII] line emission and colors significantly bluer than PLE models.

IR imaging has made it attractive to pursue gEs at redshifts $z > 1$. In the HDF-N, Zepf (1997) and Franceschini et al (1998) used ground-based *K*-band data, selecting samples by color and morphology, respectively, and concluded that there was an absence of the very red galaxies that would be expected if the elliptical population as a whole formed at very large redshift and evolved passively. In particular, Franceschini et al highlighted the apparently sudden disappearance of HDF ellipticals beyond $z > 1.3$, which suggests that either dust obscuration during early star formation, or morphological perturbation during early mergers, was responsible. Barger et al (1999) made an IR study of the HDF-N flanking fields, selecting objects by color without reference to morphology. To $K \approx 20$, they found few galaxies with $I - K > 4$, the expected color threshold for old ellipticals at $z \gg 1$. However, other comparably deep and wide IR surveys have reported substantially larger surface densities of $I - K > 4$ galaxies (Eisenhardt et al 1998; McCracken et al 2000), raising concerns about field-to-field variations. Menanteau et al (1999) studied the optical-to-IR color distribution for a sample of ∼300 morphologically early-type galaxies selected from 48 WFPC2 fields, including the HDF-N and flanking fields. They too find an absence of very red objects and a generally poor agreement with predictions from purely passive models with high formation redshifts, although the sky surface density agrees reasonably well with the sorts of models that matched the older MDS and HDF counts, i.e. those with a suitably tuned local LF.

On HST, NICMOS has provided new opportunities to identify and study ellipticals at $z \gtrsim 1$. Its small field of view, however, has limited the solid angle surveyed. Spectroscopic confirmation of the very faint, very red elliptical candidates identified so far will be exceedingly difficult, but would be well worth the effort. Treu et al (1998), Stiavelli et al (1999) and Benítez et al (1999) noted several very red, $R^{1/4}$-law galaxies in the HDF-S NICMOS field, identifying them as ellipticals at $1.4 \lesssim z_{\rm phot} \lesssim 2$. Given the small solid angle of that image, this suggests a large space density, and Benítez et al (1999) have proposed that most early type galaxies have therefore evolved only passively since $z \sim 2$. Comparably red, spheroidal galaxies are found in the NICMOS map of the HDF-N (Dickinson et al 2000a), with photometric redshifts in the range $1.2 \lesssim z \lesssim 1.9$. Their space density appears to be well below that of HDF ellipticals with similar luminosity at $z < 1.1$, in broad agreement with Zepf (1997) and Franceschini et al (1998), although the comparison to $z = 0$ is again limited primarily by uncertainties in the local gE LF. Curiously, few fainter objects with similar colors are found in the HDF-N, although the depth of the NICMOS images is adequate to detect red ellipticals with $L \sim 0.1\,L^*$ out to $z \approx 2$. Treu & Stiavelli (1999) find that PLE models with high

($z \sim 5$) and low ($z \sim 2$) formation redshifts over- and under-predict the observed counts, respectively, of red elliptical-like objects in 23 other NICMOS fields.

The HDF-N NICMOS images from Dickinson et al (2000a) and Thompson et al (1999) are deep enough to have detected red, evolved elliptical galaxies out to at least $z \sim 3$ if they were present, eliminating concerns about invisibility because of *k*-corrections (e.g. Maoz 1997). The only plausible $z > 2$ candidate is an HDF-N "*J*-dropout" object, whose colors resemble those of a maximally old gE at $z \sim 3$ (Lanzetta et al 1998; Dickinson et al 2000b; Lanzetta et al 1999). Other $z > 2$ HDF objects which some authors have morphologically classified as ellipticals (cf. Fasano et al 1998) are blue, mostly very small, manifestly star-forming "Lyman break" objects. Few if any appear to be passively evolving objects that have ceased forming stars, so the connection to present-day ellipticals is more speculative.

The collective evidence surveyed above suggests that mature, gE galaxies have been present in the field since $z \sim 1$ with space densities comparable to that at the present era. At $0.4 < z < 1$, however, they exhibit an increasingly broad range of colors and spectral properties, which suggests a variety of star formation histories over the proceeding few billion years (or alternatively errors in classification). The statistics seem to favor a substantial decline in their space density at $z \gg 1$, although the well-surveyed sightlines are small and few, and clustering might (and in fact, apparently does) cause large variations from field to field. Therefore, the conclusion has not been firmly established. Moreover, it is very difficult to achieve uniform selection at all redshifts, regardless of the criteria used (photometric, morphological, or both), and the existing samples of objects with spectroscopic (or at least well-calibrated photometric) redshifts are still small. Thus even the deceptively simple task of comparing elliptical galaxy evolution to the simple PLE hypothesis remains a stubborn challenge.

5.4 Obscured Populations

ISO and SCUBA observations of the HDF and other fields have revealed an energetically important population of dust-obscured objects. Interpretation of these results has been the subject of considerable debate, because of ambiguities in source identification and in distinguishing starbursts from AGN. The ISOCAM (6.7 and 15 μm) and SCUBA (850 μm) observations bracket but do not sample the wavelength regime $100 < \lambda_p < 200\,\mu$m near the peak of the far-IR emission, making it difficult to assess reliably the source contribution to the global emissive energy budget of galaxies. Although strong mid-IR emission accompanies vigorous star formation in many nearby galaxies, the unidentified IR emission bands carry most of the energy in the wavelength range sampled by ISOCAM at $z \sim 1$. The bulk of re-emitted radiation, however, emerges near λ_p, and there is considerable diversity in $f(10\,\mu\text{m})/f(100\,\mu\text{m})$ flux ratios among nearby luminous and ultraluminous IR galaxies. Therefore, deriving star-formation rates from mid-IR measurements alone requires a substantial extrapolation and is quite uncertain. SCUBA 850 μm observations sample the re-radiated thermal emission directly, but at a wavelength

well past λ_p, again requiring an extrapolation to total far-IR luminosities assuming a dust temperature and emissivity that are almost never well constrained by actual, multi-wavelength measurements. Furthermore, SCUBA and ISO do not in general detect the same sources. ISO detects objects out to $z \sim 1$, whereas most of the SCUBA sources could be at much higher redshifts. For both mid-IR and sub-millimeter sources, AGN-heated dust may also play a role. Several active galaxies (including radio ellipticals) in the HDF are detected by ISO, and some SCUBA sources (not yet in the HDF, however) have been identified with AGN. Chandra X-ray observations (Hornschemeier et al 2000) do not detect with high significance any of the sub-millimeter sources in the HDF.

Difficulties in identifying the optical counterparts to the mid-IR and sub-millimeter sources are a second source of ambiguity. The mean separation between galaxies in the HST images of the HDF is about $3''$. In comparison the ISO 15 μm PSF has full-width at half max (FWHM) $\approx 9''$, whereas the SCUBA 850 μm beam size is $\approx 15''$. Nevertheless, the HDF mid-IR sources have plausible counterparts among the brighter galaxies in the survey. SCUBA sources, on the contrary, often seem to have extremely faint, and sometimes entirely invisible, counterparts in the optical and near-infrared. Sub-mm objects sometimes correspond to microjansky radio sources at centimeter wavelengths, and sometimes have faint, very red near-IR counterparts. Many, however, do not, even with the deepest radio and near-IR data available with current instrumentation (see Section 4.7).

Other than the occasional ultra-red optical counterpart (of which there are none in the HDF-N), the non-AGN counterparts to sub-millimeter and far-IR sources rarely have particularly unusual photometric or spectral features which highlight them as the remarkable objects they must be. Counterparts to 6.7 and 15 μm ISO sources show a predominance of "post-starburst" Balmer absorption spectra (Flores et al 1999a,b; Aussel et al 1999b; Cohen et al 2000); apart from the occasional AGN, few have strong emission line spectra, which suggests the most intense star-forming regions are highly obscured. There are hints that the Lyman-break galaxies represent the faint tail of the sub-millimeter source population. Chapman et al (1999) detect 1 out of 18 galaxies in a targeted study of $z \sim 3$ Lyman-break galaxies. Peacock et al (1999) find a significant statistical correlation of Lyman-break galaxies with sky fluctuations in the HDF-N SCUBA map. A straightforward analysis suggests that the ratio of hidden star formation to star formation directly measured in the UV is about 6:1, and that Lyman-break galaxies account for at least 25% of the 850 μm background.

Given the present status of faint sub-millimeter and mid-IR surveys, the most telling information comes not from individual source identifications but from the ensemble statistics using the combined data from many surveys. The ISO 15 μm number counts show good agreement between various surveys and a strong excess over no-evolution models (Elbaz et al 1999), as do 850 μm SCUBA counts (Barger et al 1999; Blain et al 1999). As with the "faint blue galaxy" excess (Kron, 1980) that helped spark the boom in the optical study of distant field galaxies in the 1970s and 1980s, the ISO and SCUBA counts point toward strong cosmological

evolution, probably manifesting the star formation history of the galaxy population. And like the faint blue galaxy problem, the robust interpretation of this number count excess will undoubtedly require extensive follow-up observations to characterize the source population and its properties. Currently, given the uncertainties in source identification, in extrapolating the current measurements to "true" far-IR luminosities, and in balancing the roles of AGN vs. star formation, it seems premature to attempt a detailed revision of our picture of galaxy evolution and cosmic star formation. But it is also abundantly clear that a true understanding will have to account for the important and perhaps dominant energetic role played by this obscured population.

5.5 Global Star-Formation History and Chemical Evolution

Interest in the integrated background light from galaxy formation is long-standing (e.g. Bondi et al 1955), and has motivated a large number of experiments aimed at measuring the diffuse extragalactic background (e.g. Spinrad & Stone 1978; Dube et al 1979; Matsumoto et al 1988; Bernstein 1997; Hauser et al 1998). Although the integrated background records the light from all galaxies, whether or not they are individually detected, the task of separating out galactic foregrounds and instrumental backgrounds is formidable, and many of the measurements are only upper limits. An alternative approach is to add up the UV emission from galaxies that are individually detected. This approach formally produces only a lower limit for the true UV luminosity density, but it provides a basis for exploring connections of the high- and low-redshift universe and for deciding which of the various selection effects are plausible and important.

The UV emission from galaxies is directly connected to their metal production (Cowie et al 1988) because the UV photons come from the same massive stars that produce most of the metals through type II SNe. The relation between UV emissivity and metal production is not strongly dependent on the initial mass function, varying by a factor of only 3.3 between the Salpeter (1955) and Scalo (1986) forms. In contrast, the relation of UV emission to the total star-formation rate is much more tenuous because the low-mass end of the IMF contains most of the mass, whereas the high-mass end produces most of the UV emission. As a result, it is easier to constrain the history of metal production in the universe than it is to constrain the overall star-formation history. Prior to the HDF, estimates of the metal-production vs. redshift, $\dot{\rho}_z(z)$ had been made from ground-based galaxy redshift surveys (Lilly et al 1996) and from QSO absorption line statistics (e.g. Lanzetta et al 1995; Pei & Fall 1995; Fall et al 1996), and the observations at the time suggested an order-of-magnitude increase in $\dot{\rho}_z(z)$ from $z = 0$ to $z = 1$.

Madau et al (1996) made the first attempt to connect the luminosity density in HDF high-redshift galaxy samples to lower-redshift surveys. The plot of the metal-formation rate vs. redshift has provided a focal point for discussion of the HDF and for comparisons to theoretical models. In the Madau et al (1996) paper, galaxies in redshift slices $2 < z < 3.5$ and $3.5 < z < 4.5$ were identified by strict

color-selection criteria that were shown via simulations to provide strong rejection of objects outside the desired redshift intervals. The luminosity of the galaxies within these redshift intervals was estimated by simply summing the observed fluxes of the galaxies, and no dust or surface-brightness corrections were applied. The results were presented as lower limits because nearly all of the corrections will drive the derived metal-formation rates up. The initial Madau et al (1996) diagram showed a metal-production rate at $z \sim 4$ that was roughly a factor of 10 lower than the rate at $z \sim 1$. Madau (1997) subsequently modified the color-selection criteria and integrated down an assumed luminosity function, revising the $z > 2$ rates upward by about a factor of 3. There was remarkable agreement between $\dot{\rho}_z(z)$ derived from the galaxy luminosities, the results of Pei & Fall (1995), and the predictions of hierarchical models (e.g. White & Frenk 1991; Cole et al 1994; Baugh et al 1998), all of which show a peak in the metal production rate at $z \sim 1-2$. Subsequent work in this area has focused on (*a*) galaxy selection (*b*) effects of dust, and (*c*) the connection of the Madau diagram to general issues of galaxy evolution and cosmic chemical evolution, which we discuss in turn.

5.5.1 Galaxy Selection The color-selection criteria of Madau et al (1996) are extremely conservative, and spectroscopic surveys (Steidel et al 1996; Lowenthal et al 1997) have identified at least a dozen $2 < z < 3.5$ galaxies with $U_{300} - B_{450} > 1.3$ but with $B_{450} - I_{814}$ redder than the Madau et al (1996) selection boundary. Alternative color-selection criteria (particularly in the $2 < z < 3.5$ range) have been explored in a number of studies (Clements & Couch, 1996; Lowenthal et al 1997; Madau et al 1998; Meurer et al 1999), with the result that the luminosity-density goes up as the area in color space is enlarged. The number of low-*z* interlopers also may go up, although spectroscopic surveys suggest that the Meurer et al (1999) selection boundary is not prone to this problem. Similar techniques have been applied to ground-based images covering much wider areas but sensitive only to brighter objects (see, e.g. Steidel et al 1999 and Giallongo et al 1998 for recent examples). Substantial progress has been made both in refining the estimates of the volume sampled by the color selection and in estimates of the high-*z* galaxy luminosity functions (Dickinson, 1998; Steidel et al 1999). These allow more precise (but more model-dependent) estimates of the luminosity density at $z > 3$. In Figure 5 we provide an updated plot of star-formation vs. redshift from the color-selected samples of Steidel et al (1999) and Casertano et al (2000), now including integration down the luminosity function and a correction for mean dust attenuation.

Photometric redshifts computed via template fitting can also be used to identify samples of high-*z* objects, and several such samples have been presented and discussed (Lanzetta et al 1996; Sawicki et al 1997; Sawicki & Yee, 1998; Mirallers & Pello, 1998; Rowan-Robinson, 1999; Fontana et al 1999). Luminosity densities at $z > 2$ from these studies are generally higher than those of Madau et al (1996), and the apparent drop in $\dot{\rho}_z(z)$ at $z \gtrsim 2$ is not universally evident. A striking example of the difference between color-selected samples and

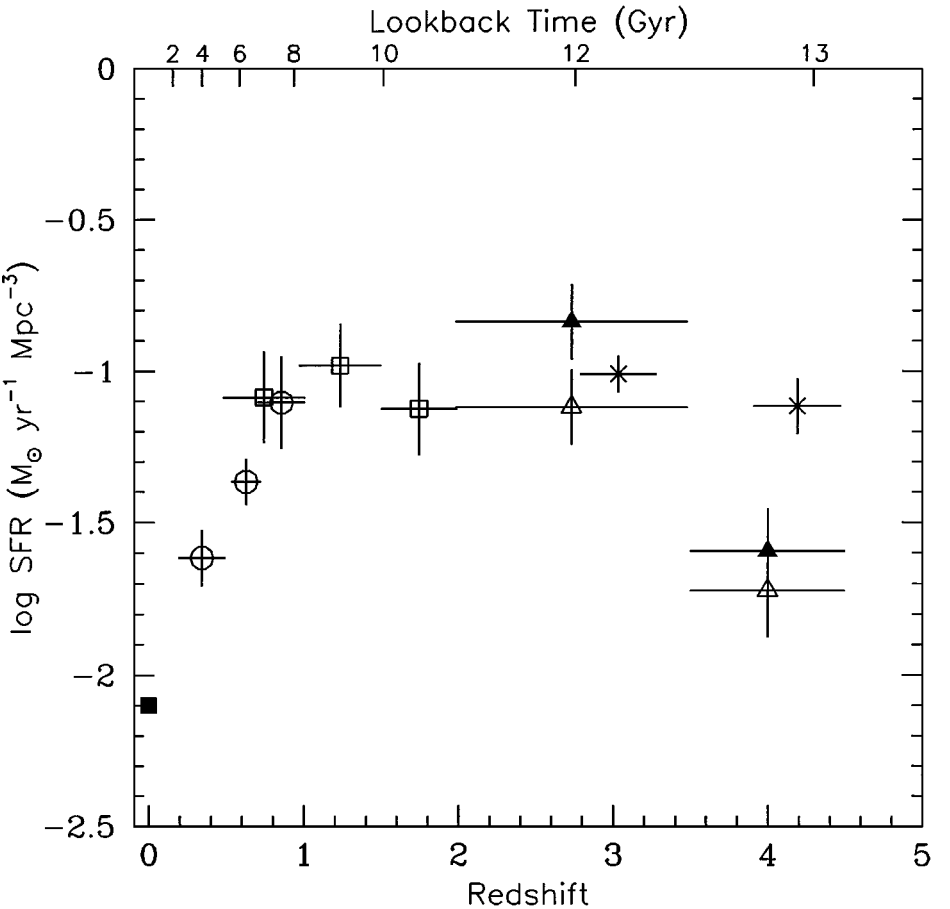

Figure 5 (left) Star-formation rate density vs. redshift derived from UV luminosity density. The $z > 2$ points are from Lyman-break objects in the HDF-N (open triangles), in the HDF-S (filled triangles) and in the Steidel et al (1999) ground-based survey (X's). The luminosity density has been determined by integrating over the luminosity function and correcting for extinction following the prescription of Steidel et al (1999). Possible contributions from far-IR and sub-millimeter sources are not included. Also not included are the upward revisions of the $z < 1$ star-formation densities suggested by Tresse & Maddox (1998) and Cowie et al (1999). For the lower-redshift points, the open squares are from HDF photometric redshifts by Connolly et al (1997), the open circles are from Lilly et al (1996), and the solid square is from the Hα survey of Gallego et al (1995).

photometric-redshift selected samples is the fact that HDF-S comes out with a higher UV luminosity-density than HDF-N in the color-selected sample shown in Figure 5, but a lower luminosity density in the photometric-redshift selected sample of Fontana et al (1999). One general concern about object selection is that galaxies at lower redshift are typically *brighter* than the high-z objects. Interlopers that make it into photometric samples can dominate the UV luminosity-density estimates.

It does appear evident that the original criteria of Madau et al (1996) were too conservative, and the *directly measured* UV luminosity density in bins at $z \sim 3$ and $z \sim 4$ is not demonstrably lower than it is at $z \sim 1$. At still higher redshifts, from the very small number of candidate objects with $z > 5$, Lanzetta et al (1998) computes an upper limit on the star-formation density at $z \sim 5 - 12$. For the cosmology adopted here, the limit on star formation in galaxies with $\dot{M} \gtrsim 100$ $h M_\odot$ yr^{-2} is lower than the inferred rate from Lyman-break galaxies at $z = 4$. With NICMOS observations it has become possible to identify $z > 5$ candidates to much fainter limits, detecting objects with UV luminosities more like those of typical Lyman-break galaxies at $2 < z < 5$. Dickinson (2000) derives number counts for color–selected candidates at $4.5 < z < 8.5$ in the HDF–N/NICMOS survey, and finds that they fall well below nonevolving predictions based on the well-characterized $z = 3$ Lyman-break luminosity function. It appears that the space density, the luminosities, or the surface brightnesses (and hence, the detectability) of UV bright galaxies fall off at $z > 5$, at least in the HDF–N.

5.5.2 Dust and Selection Effects Many of the discussions of the Madau diagram have centered around selection effects and whether the data actually support a decrease in $\dot{\rho}(z)$ for $z \gtrsim 2$. Star formation in dusty or low-surface-brightness galaxies may be unaccounted for in the HDF source counts. Meurer and collaborators (Meurer et al 1997, 1999) use local starburst galaxy samples to calibrate a relation between UV spectral slope and far-IR (60–100 μm) emission, and hence compute bolometric corrections for dust attenuation. They apply these corrections to a sample of color-selected Lyman-break galaxies in the HDF and derive an absorption-corrected luminosity density at $z \sim 3$ that is a factor of 9 higher than that derived by Madau et al (1996). Not all of this comes from the dust correction; the luminosity-weighted mean dust-absorption factor for the Meurer et al (1999) sample is 5.4 at 1600 Å. Sawicki & Yee (1998) analyzed the optical/near-IR spectral energy distributions of spectroscopically confirmed Lyman-break galaxies in the HDF and found the best fit synthetic spectra involved corrections of more than a factor of 10. Smaller corrections were derived by Steidel et al (1999) for a sample of galaxies of similar luminosity. In general, the danger of interpreting UV spectral slopes as a measure of extinction is that the inferred luminosity corrections are very sensitive to the form of the reddening law at UV wavelengths. For the Calzetti et al (1994) effective attenuation law, used in most of the aforementioned studies, a small change in the UV color requires a large change in the total extinction. Photometric errors also tend to increase the dust correction, because

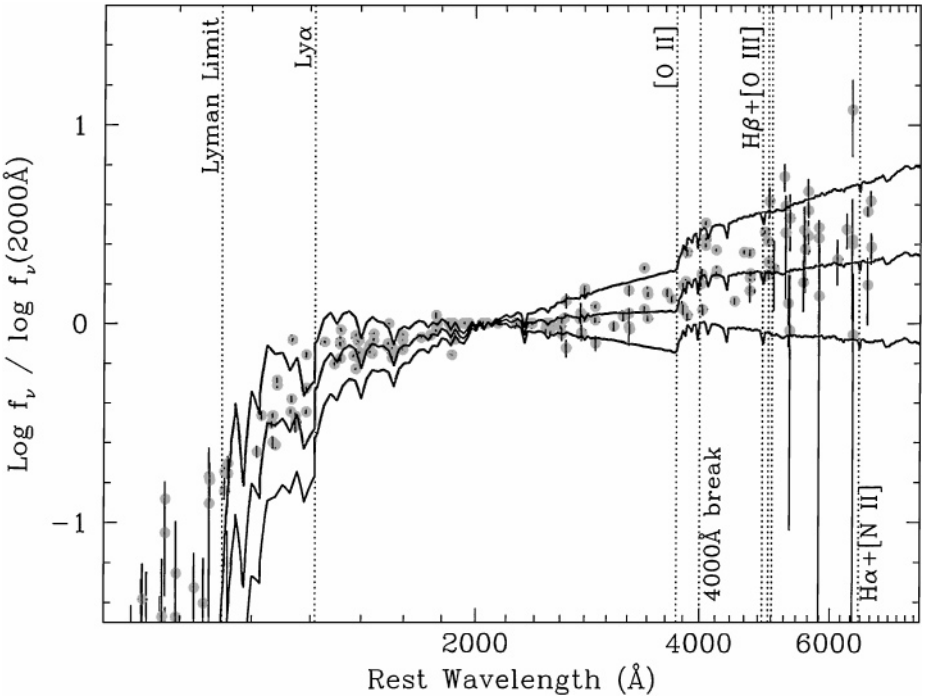

Figure 6 Spectral energy distributions of 28 spectroscopically confirmed Lyman-break galaxies with $2.5 < z < 3.5$, corresponding to a lookback time ∼12 billion years, superimposed on stellar population models. The models assume solar metallicity and a Salpeter IMF and include attenuation due to the IGM for $z = 3$. The models reflect constant star formation for 10^9 years, with different amounts of interstellar dust attenuation. The reddening values are $E(B-V) = 0$, 0.2, and 0.4, with the curve that is highest at long wavelengths having the highest value. The Calzetti et al (1994) attenuation law was used.

objects that scatter to the red are assigned larger corrections that are not offset by smaller corrections for the blue objects. The corrections for dust must thus be regarded as tentative, and must be confirmed with more extensive Hα studies such as that of Pettini et al (1998) and further studies in the mid-IR, radio, and sub-millimeter.

The NICMOS HDF observations provide some additional insight into possible reddening corrections. Figure 6 shows the spectral-energy distributions of HDF galaxies with spectroscopic $2.5 < z < 3.5$, superimposed on models with a constant star-formation rate and an age of 10^9 years. The galaxies are typically best fitted with ages 10^{7-9} years and reddening $0.1 < E(B-V) < 0.4$ with the Calzetti et al (1994) attenuation law. Very young galaxies with little extinction appear to be rare, and older or more reddened galaxies would possibly escape the Lyman-break selection. However, Ferguson (1999) identified only 12 galaxies with

$V_{606} < 27$ in the HDF-N that fail the Dickinson (1998) color criteria but nevertheless have $2.5 < z_{\rm phot} < 3.5$ from spectral-template fitting. In general these galaxies fall just outside the color selection boundaries, and the non-dropout sample contributes only 12% of the luminosity-density of the dropout sample. It thus appears unlikely that there is a population that *dominates* the metal-enrichment rate at $z \sim 3$ that is just missing from the Lyman-break samples. If the optically unidentified sub-millimeter sources (see Section 4.7) are really at $z \gtrsim 3$, they are probably a disjoint population, rather than simply the red tail of the Lyman-break population.

If sources akin to ultra-luminous IRAS galaxies were present at $z \sim 3$ in the HDF, it is likely that they would be detected, but unlikely that they would be identified as Lyman-break galaxies. Trentham et al (1999) use HST observations to extend the spectral energy distributions for three nearby ultra-luminous IR galaxies down to rest-frame 1400 Å. Although this is not far enough into the UV to predict HDF B_{450} colors at $z = 3$ with confidence, it at least gives some indication of whether such galaxies are detectable. All three galaxies would likely be detected in the $F814W$ band if shifted out to $z = 3$, although VII Zw 031 would be very near the detection limit. None of the galaxies would meet the Madau et al (1996) Lyman-break galaxy selection criteria, but some might plausibly show up as high-z objects from their photometric redshifts.

In addition to dust, cosmological surface-brightness can bias the samples of high-redshift galaxies. For fixed luminosity and physical size, i.e. no evolution, surface brightness will drop by about 1 mag between $z = 3$ and $z = 4$. This lower surface brightness will result in a decrease in the number density of objects and the inferred luminosity density, even if there is no intrinsic evolution. Using simulated images for one particular galaxy evolution model (Ferguson & Babul, 1998), Ferguson (1998b) arrived at corrections to $\dot{\rho}_z(z)$ of a factor of 1.5 at $z \sim 3$ and 4.7 at $z \sim 4$. Lanzetta et al (1999) have looked at surface-brightness selection in a less model-dependent way, computing the star-formation "intensity" (in solar masses per year per square kiloparsec) from the UV flux in each pixel of the galaxy images. The comoving volume density of the regions of highest star-formation intensity appears to increase monotonically with increasing redshift, whereas a strong selection cutoff for star-formation intensities less than 1.5 $M_\odot$ yr^{-1} kpc^{-2} affects samples beyond $z > 2$. The results suggest that surface-brightness effects produce a substantial underestimate of $\dot{\rho}_z(z)$ at high redshift.

The undetected low-surface-brightness, UV-emitting regions should contribute to the total diffuse background in the image. Bernstein (1997) has attempted to measure the mean level of the extragalactic background light (EBL) in the HDF images, while Vogeley (1997) has analyzed the autocorrelation function of the residual fluctuations after masking the galaxies. Vogeley (1997) concludes that diffuse light clustered similarly to faint galaxies can contribute no more than $\sim$20% of the mean EBL. In contrast Bernstein (1997) concludes that the total optical EBL is two to three times the integrated flux in published galaxy counts. The two results can be made marginally compatible if the fluxes of detected galaxies are

corrected for light lost outside the photometric apertures and for oversubtraction of background due to the overlapping wings of galaxy profiles. If this interpretation is correct, there is not much room for the UV luminosity density to increase significantly at high redshift.

5.5.3 Connection to Galaxy Evolution An important use of the metal-enrichment rate derived from the HDF and other surveys is the attempt to "close the loop": to show that the emission history of the universe produces the metal abundances and stellar population colors we see at $z \sim 0$. Madau et al (1996) made a first attempt at this, concluding that the metals we observe being formed [integrating $\dot{\rho}_z(z)$ over time] are a substantial fraction of the entire metal content of galaxies.

Madau et al (1998) compared the integrated color of galaxy populations in the local universe to that expected from the UV-emission history, exploring a variety of options for IMF and dust obscuration. With a Salpeter IMF and modest amounts of dust attenuation, they find that a star-formation history that rises by about an order of magnitude from $z = 0$ to a peak at $z \sim 1.5$ is compatible with the present-day colors of galaxies, with the FIR background, and with the metallicities of damped Lyα absorbers. Fall et al (1996), Calzetti & Heckman (1999) and Pei et al (1999) have attempted to incorporate dust and chemical evolution in a more self-consistent way. The models include a substantial amount of obscured star formation; more than 50% of the UV radiation is reprocessed by dust. The obscuration corrections increase the value of $\dot{\rho}_z(z)$ from samples already detected in optical surveys, but do not introduce whole classes of completely dust-obscured objects. Although there are significant differences in the inputs and assumptions of the models, in all cases a model with a peak in $\dot{\rho}_z(z)$ at $z \sim 1 - 1.5$ is found consistent with a wide variety of observations. In particular the models can simultaneously fit the COBE DMR and FIRAS measurements of the cosmic IR background (Puget et al 1996; Hauser et al 1998; Fixsen et al 1998) and the integrated light from galaxy counts. The total mass in metals at $z = 0$ is higher in these new models than in those of Madau et al (1996), but the local census now includes metals in cluster X-ray gas, which were ignored by Madau et al (1996).

Overall, the success of these consistency checks is quite remarkable. Various imagined populations of galaxies (dwarfs, low-surface-brightness galaxies, highly dust-obscured objects, etc.) now seem unlikely to be cosmologically dominant. The fact that the UV emission, gas metallicities, and IR backgrounds all appear capable of producing a universe like the one we see today leaves little room for huge repositories of gas and stars missing from either our census at $z = 0$ or our census at high redshift.

Nonetheless, there is room for caution in this conclusion. In clusters of galaxies, the mass of metals ejected from galaxies into the X-ray–emitting gas exceeds that locked inside stars by a factor of 2–5 (Mushotzky & Loewenstein, 1997). If the same factor applies to galaxies outside clusters (Renzini, 1997), then the local mass-density of metals greatly exceeds the integral of the metal-enrichment rate, implying that *most* star-formation is hidden from the UV census (although the

differences in galaxy morphology in clusters and in the field suggests that clusters might not be typical regions of the universe). Various lines of evidence cited in Section 5.3 point to old ages for elliptical galaxies (both inside and outside of clusters) and the bulges of luminous early-type spirals (Renzini, 1999; Goudfrooij et al 1999). The requirements for the early formation of metals in these systems look to be at odds with the inferences from the models described above. Renzini (1999) estimates that 30% of the current density of metals must be formed by $z \sim 3$, whereas the best-fit models to the evolution of the luminosity density have only 10% formed by then. The discrepancy is interesting but is not outside of the range of error of the estimates of both $\dot{\rho}_z(z)$ and the ages of stellar populations in present-day spheroidal systems.

It also remains a challenge to ascertain how the metals got from where they are at high redshift to where they are today. The bulk of the metals locked up in stars at $z = 0$ are in luminous, normal, elliptical, and spiral galaxies. If elliptical galaxies (and spheroids in general) formed early and rapidly, they probably account for the lion's share of $\dot{\rho}_z(z)$ above $z = 2$. Thus the metals formed in the $z = 1$ peak of $\dot{\rho}_z(z)$ must end up for the most part in luminous spiral galaxies today. This is difficult to reconcile with the lack of evolution observed in number density or luminosity of luminous spirals out to $z = 1$. An order-of-magnitude decline in star-formation rate in galaxy disks since $z = 1$ also seems inconsistent with present-day colors of spiral galaxy disks, or with star-formation histories derived from chemical-evolution models (e.g. Tosi 1996; Prantzos & Silk 1998). Furthermore, at $z \sim 1$ it appears that compact-narrow-emission-line galaxies (Guzman et al 1997) and irregular galaxies account for a significant fraction of the UV luminosity density. If these galaxies fade into obscurity today, then they have not been accounted for in the census of metals in the local universe, and the $z = 0$ metallicity should be revised upwards in the global chemical-evolution models. On the other hand, if these galaxies are merging into luminous spirals and ellipticals, it is hard to understand how luminous spiral and elliptical galaxy properties can remain consistent with PLE models out to $z = 1$.

5.6 Clustering of High-Redshift Galaxies

Until relatively recently, evolution of the spatial two-point correlation function ξ has typically been modeled as a simple power-law evolution in redshift

$$\xi(r, z) = (r_0/r)^{\gamma}(1+z)^{-(3+\epsilon-\gamma)}, \tag{3}$$

where r and r_0 are expressed in comoving coordinates (e.g. Groth & Peebles 1977). For $\epsilon = 0$, the formula above corresponds to stable clustering (fixed in proper coordinates), while for $\epsilon = \gamma - 3$, it corresponds to a clustering pattern that simply expands with the background cosmology. Although these two cases may bound the problem at relatively low redshift, the situation becomes much more complex as galaxy surveys probe to high redshifts. In particular, the complex merging and fading histories of galaxies make it unlikely that such a simple formula could

hold, and the differences in sample selection at high- and low-z make it unclear whether the analysis is comparing the same physical entities. In practice it is likely that galaxies are biased tracers of the underlying dark-matter distribution, with a bias factor b that is non-linear, scale-dependent, type-dependent, and stochastic (Magliocchetti et al 1999; Dekel & Lahav 1999).

In hierarchical models, the correlation function $\xi(r)$ of halos on linear scales is given by the statistics of peaks in a Gaussian random field (Bardeen et al 1986). Peaks at a higher density threshold $\delta\rho/\rho$ have a higher correlation amplitude, and their bias factor b, relative to the overall mass distribution, is completely specified by the number density of peaks (e.g. Mao & Mo 1998).

The comparison of the clustering of high-redshift galaxies in the HDF and in ground-based surveys provides a strong test of whether there is a one-to-one correspondence between galaxies and peaks in the underlying density field. The bias factor observed in Lyman-break samples (Steidel et al 1998; Adelberger et al 1998; Giavalisco et al 1998) is in remarkable agreement with the expectations from such a one-to-one correspondence. As the luminosity of Lyman-break galaxies decreases, the number density increases, and the clustering amplitude decreases (Giavalisco et al 2000). These trends are all in agreement with a scenario in which lower-luminosity Lyman-break galaxies inhabit lower-mass halos. Thus, at redshifts $z \sim 3$, the connection between galaxies and dark matter halos may in fact be quite simple and in good agreement with theoretical expectations.

The picture becomes less clear for the samples described in Section 4.12. In particular, the interpretation of the apparent evolution in the correlation length r_0 or the bias factor b from the Magliocchetti & Maddox (1999) and Arnouts et al (1999) studies involves a sophisticated treatment of the merging of galaxies and galaxy halos over cosmic time. Fairly detailed attempts at this have been made using either semi-analytic models (Baugh et al 1999; Kauffmann et al 1999) or more generic arguments (e.g. Matarrese et al 1997; Moscardini et al 1998; Magliocchetti et al 1999, following on earlier work by Mo & Fukugita 1996, Mo & White 1996, Jain 1997, Ogawa et al 1997 and others). These studies all assume that galaxy mass is directly related to halo mass, which may not be true in reality at lower z, but which is an assumption worth testing. A generic prediction of the models is that the effective bias factor (the value of b averaged over the mass function) should increase with increasing redshift. The correlation length r_0 is relatively independent of redshift (to within a factor of $\sim$3), in contrast to the factor of $\sim$10 decline from $z = 0$ to $z = 4$ predicted for non-evolving bias. The results shown by Arnouts et al (1999) are qualitatively consistent with this behavior. However, it is worth re-emphasizing that the HDF is a very small field. The standard definition for the bias factor b is the ratio of the root mean square density fluctuations of galaxies relative to mass on a scale of $8\ h^{-1}$ Mpc. Fluctuations on this angular scale clearly have *not* been measured in the HDF, and the interpretation rests on (*a*) the assumption of a power-law index $\gamma = 1.8$ for the angular correlation function (which is not in fact predicted by the models) (Moscardini et al 1998), and (*b*) the

fit to the integral constraint. Clearly much larger areas are needed before secure results can be obtained.

Roukema & Valls-Gabaud (1997) and Roukema et al (1999) point out that much of the measured clustering signal in the HDF comes from scales 25–250 kpc, which is within the size of a typical L^* galaxy halo at $z = 0$. The connection of the observed correlation function to hierarchical models thus depends quite strongly on what happens when multiple galaxies inhabit the same halo. Do they co-exist for a long time (e.g. as in present-day galaxy groups and clusters), or rapidly merge together to form a larger galaxy (in which case one should consider a "halo exclusion radius" in modeling the correlation function)? As the halo exclusion radius increases, the predicted correlation amplitude on scales of $5''$ decreases relative to the standard cosmological predictions. The slope of $\omega(\theta)$ also differs from $\gamma = 1.8$ for $\theta\, z \lesssim 20''$. Roukema et al (1999) find that the HDF data for $1.5 < z_{\rm phot} < 2.5$ are best fit with stable clustering, a halo-exclusion radius of $r_{\rm halo} = 200\, h^{-1}$ kpc, and a low-density universe.

6. CONCLUSION

The HDFs represent an important portion of the frontier in studies of the distant universe. Although we can point to few problems that were solved by the HDF alone, the HDF has contributed in a wide variety of ways to our current understanding of distant galaxies and to shaping the debate over issues such as the origin of elliptical galaxies and the importance of obscured star formation. The scientific impact of the HDF can be attributed in part to the wide and nearly immediate access to the data. The fact that many groups and observatories followed this precedent (both for HDF data and subsequently for data from other surveys) illustrates that a deeper understanding of the universe will come not from any one set of observations but from sharing and comparing different sets of observations. Not all kinds of surveys are amenable to this kind of shared effort, but the precedent set by the HDF in the social aspects of carrying out astronomical research may ultimately rival its significance in other areas.

ACKNOWLEDGMENTS

We are indebted to our fellow HDF enthusiasts, too numerous to mention, for the many fruitful discussions that have provided input for this review. The observations themselves would not have happened without the dedicated contribution from the HST planning operations staff, to whom we owe the largest debt of gratitude. This work was based in part on observations with the NASA/ESA Hubble Space Telescope obtained at the Space Telescope Science Institute, which is operated by the Association of Universities for Research in Astronomy, Inc., under NASA contract NAS5-26555. This work was partially supported by NASA grants GO-07817.01-96A and AR-08368.01-97A.

LITERATURE CITED

Abraham RG. 1997. In *The Ultraviolet Universe at Low and High Redshift: Probing the Progress of Galaxy Evolution*, ed. WH Waller, MN Fanelli, JE Hollis, AC Danks, P. 195. Woodbury, New York: AIP

Abraham RG, Ellis RS, Fabian AC, Tanvir NR, Glazebrook K. 1999a. *MNRAS* 303:641

Abraham RG, Merrifield MR, Ellis RS, Tanvir NR, Brinchmann J. 1999b. *MNRAS* 308:569

Abraham RG, Tanvir NR, Santiago BX, Ellis RS, Glazebrook K, van den Bergh S. 1996. *MNRAS* 279:L47

Adelberger KL, Steidel CC, Giavalisco M, Dickinson M, Pettini M, Kellogg M. 1998. *Ap. J.* 505:18

Alcock C, Allsman RA, Alves D, Axelrod TS, Becker AC, et al. 1997. *Ap. J.* 486:697

Almaini O, Fabian A. 1997. *MNRAS* 288:L19

Aragón-Salamanca A, Ellis RS, Couch WJ, Carter D. 1993. *MNRAS* 262:764

Arnouts S, Cristiani S, Moscardini L, Matarrese S, Lucchin F, et al. 1999. *MNRAS* 310:540

Aussel H, Cesarsky CJ, Elbaz D, Starck JL. 1999a. *Astron. Astrophys.* 342:313

Aussel H, Elbaz D, Cesarsky CJ, Starck JL. 1999b. In *The Universe as Seen by ISO*, ed. P Cox MF Kessler, p. 1023. Noordwijk: ESA

Babul A, Ferguson HC. 1996. *Ap. J.* 458:100

Babul A, Rees M. 1992. *MNRAS* 255:346

Bahcall JN, Guhathakurta P, Schneider DP. 1990. *Science* 248:178

Bardeen JM, Bond JR, Kaiser N, Szalay AS. 1986. *Ap. J.* 304:15

Barger AJ, Cowie LL, Richards EA. 1999. In *Photometric Redshifts and the Detection of High-Redshift Galaxies*, ed. R Weymann, L Storrie-Lombardi, M Sawicki, & R Brunner, p. 279. San Francisco: ASP

Barger AJ, Cowie, LL, Sanders, DB. 1999. *Ap. J. Lett.* 518:L5

Barger AJ, Cowie LL, Sanders DB, Fulton E, Taniguchi Y, et al. 1998. *Nature* 394:248

Barger AJ, Cowie LL, Trentham N, Fulton E, Hu EM, et al. 1999. *Astron. J.* 117:102

Barkana R, Blandford R, Hogg DW. 1999. *Ap. J. Lett.* 513:L91

Baugh C, Benson AJ, Cole S, Frenk CS, Lacey CG. 1999. *MNRAS* 305:21

Baugh CM, Cole S, Frenk CS. 1996. *MNRAS* 282:L27

Baugh CM, Cole S, Frenk CS, Lacey CG. 1998. *Ap. J.* 498:504

Benítez N, Broadhurst T, Bouwens R, Silk J, Rosati P. 1999. *Ap. J.* 515:65

Bergeron J, Petitjean P, Cristiani S, Arnouts S, Bresolin F, Fasano G. 1999. *Astron. Astrophys.* 343:L40

Bernstein R. 1997. "*The HST/LCO Measurement of the Mean Flux of the Extragalactic Background Light (3000–8000 Å).*" PhD. Thesis. California Institute of Technology

Bershady MA. 1997. In *Dark and Visible Matter in Galaxies. ASP Conf. Ser.* 117, ed. M Persic & P Salucci, p. 537. ASP

Bershady MA, Lowenthal JD, Koo DC. 1998. *Ap. J.* 505:50

Bertin E, Arnouts S. 1996. *Astron. Astrophys. Suppl.* 117:393

Blain AW, Kneib JP, Ivison RJ, Smail I. 1999. *Ap. J. Lett.* 512:L87

Blandford R. 1998. In *The Hubble Deep Field: STScI Symposium Ser. 11*, ed. M Livio, SM Fall, & P Madau, p. 245. Cambridge: Cambridge Univ. Press

Bohlin RC, Cornett R, Hill JK, Hill RS, Landsman WB, et al. 1991. *Ap. J.* 368:12

Bondi H, Gold T, Hoyle F. 1955. *Observatory* 75:80

Bouwens R, Broadhurst T, Silk J. 1997. astro-ph/9710291

Budavari T, Szalay AS, Connolly AJ, Csabai I, Dickinson M. 1999. In *Photometric Redshifts and the Detection of High-Redshift Galaxies*, ed. R Weymann, L Storrie-Lombardi, M

Sawicki, & R Brunner, p. 19., San Francisco: ASP
Calzetti D, Heckman TM. 1999. *Ap. J.* 519:27
Calzetti D, Kinney AL, Storchi-Bergmann T. 1994. *Ap. J.* 429:582
Campos A. 1997. *Ap. J.* 488:606
Campos A, Shanks T. 1997. *MNRAS* 291:383
Carilli CL, Yun MS. 1999. *Ap. J. Lett.* 511:L13
Casertano S, de Mello D, Ferguson HC, Fruchter AS, Gonzalez RA, et al. 2000, *Astron. J.* Submitted
Casertano S, Ratnatunga KU, Griffiths RE, Im M, Neuschaefer LW, et al. 1995. *Ap. J.* 453:599
Chabrier G, Mera D. 1997. *Astron. Astrophys.* 328:83
Chapman SC, Scott D, Steidel CC, Borys C, Halpern M, et al. 1999, submitted
Chen HW, Lanzetta KM, Pascarelle S. 1999. *Nature* 398:586
Clements DL, Couch WJ. 1996. *MNRAS* 280:L43
Cohen JG. 1999. astro-ph/9910242
Cohen JG, Cowie LL, Hogg DW, Songaila A, Blandrod R, et al. 1996. *Ap. J. Lett.* 471:L5
Cohen JG, Hogg DW, Blandford R, Cowie LL, Hu EM, et al. 2000, submitted
Cole S, Aragon-Salamanca A, Frenk CS, Navarro JF, Zepf SE. 1994. *MNRAS* 271:781
Colley W, Gnedin O, Ostriker JP, Rhoads JE. 1997. *Ap. J.* 488:579
Colley WN, Rhoads JE, Ostriker JP, Spergel DN. 1996. *Ap. J. Lett.* 473:L63
Connolly AJ, Szalay AS, Brunner RJ. 1999. *Ap. J. Lett.* 499:L125
Connolly AJ, Szalay AS, Dickinson M, SubbaRao MU, Brunner RJ. 1997. *Ap. J.* 486: 11
Conselice CJ, Bershady MA, Jangren A. 1999. ApJ, in press (astro-ph/9907399)
Conselice CJ, Bershady MD, Dickinson M, Ferguson HC, Postman M, et al. 2000, in preparation
Conti A, Kennefick JD, Martini P, Osmer PS. 1999. *Astron. J.* 117:645
Cooray A, Quashnock JM, Miller MC. 1999. *Ap. J.* 511:562
Couch WJ. 1996. http://ecf.hq.eso.org/hdf/catalogs/
Cowie LL, Barger A. 1999. astro-ph/9907043
Cowie LL, Hu EM, Songaila A. 1995a. *Nature* 377:603
Cowie LL, Hu EM, Songaila A. 1995b. *Astron. J.* 110:1576
Cowie LL, Lilly SJ, Gardner JP, McLean IS. 1988. *Ap. J. Lett.* 332:L29
Cowie LL, Songaila A. 1996. Hawaii Active Catalog http://www.ifa.hawaii.edu/∼cowie/tts/tts.html
Cristiani S. 1999. *Formation and Evolution of Galaxies*, Proc. 1st Workshop of the Italian Netw., In press (astro-ph/99008165)
de Jong RS, Lacey C. 1999. astro-ph/9910066
De Propris R, Stanford SA, Eisenhardt PR, Dickinson M, Elston R. 1999. *Astron. J.* 118:719
Dekel A, Lahav O. 1999. *Ap. J.* 520:24
Dell'Antonio IP, Tyson JA. 1996. *Ap. J. Lett.* 473:L17
Dennefeld M, et al. 2000, in preparation
Désert FX, Puget JL, Clements DL, Pérault M, Abergel A, et al. 1999. *Astron. Astrophys.* 342:363
Dickinson M. 1995. In *Galaxies in the Young Universe*, ed. H Hippelein, HJ Meisenheimer, & HJ Röser, p. 144. Berlin: Springer
Dickinson M. 1998. In *The Hubble Deep Field*, ed. M Livio, SM Fall, & P Madau, p. 219. Cambridge: Cambridge University Press
Dickinson M. 2000. Philosophical Transactions of the Royal Society, Series A, in press.
Dickinson M, et al. 2000a, in preparation
Dickinson M, Hanley C, Elston R, Eisenhardt PR, Stanford SA, et al. 2000b. *Ap. J.* 531:624
Djorgovski S, Soifer BT, Pahre MA, Larkin JE, Smith JD, et al. 1995. *Ap. J. Lett.* 438:L13
Downes D, Neri R, Greve A, Guilloteau S, Casoli F, et al. 1999. *Astron. Astrophys.* 347:809
Dressler A, Oemler AJ, Sparks WB, Lucas RA. 1994. *Ap. J. Lett.* 435:L23
Driver SP. 1999. astro-ph/9909469
Driver SP, Fernández-Soto A, Couch WJ, Odewahn SC, Windhorst RA, et al. 1998. *Ap. J. Lett.* 496:L93

Driver SP, Windhorst RA, Griffiths RE. 1995. *Ap. J.* 453:48

Driver SP, Windhorst RA, Ostrander EJ, Keel WC, Griffiths RE, Ratnatunga KU. 1995. *Ap. J. Lett.* 449:L23

Dube RR, Wickes WW, Wilkinson DT. 1979. *Ap. J.* 232:333

Efstathiou G. 1992. *MNRAS* 256:43P.

Efstathiou G, Bernstein G, Tyson JA, Katz N, Guhathakurta P. 1991. *Ap. J.* 380:L47

Eggen OJ, Lynden-Bell D, Sandage A. 1962. *Ap. J.* 136:748

Eisenhardt P, Elston R, Stanford SA, Dickinson M, Spinrad H, et al. 1998. In *Xth Rencontres de Blois: The Birth of Galaxies*, ed. B Guiderdoni, F Bouchet, TX Thuan, & JTT Van. Paris: Edition Frontieres, in press

Elbaz D, Aussel H, Cesarsky CJ, Desert FX, Fadda D, et al. 1999. In *The Universe as Seen by ISO*, ed. P Cox & MF Kessler, p. 999. Noordwijk: ESA

Ellis RS. 1997. *ARAA* 35:389

Ellis RS, Smail I, Dressler A, Couch WJ, Oemler A, et al. 1997. *Ap. J.* 483:582

Elson RAW, Santiago BX, Gilmore GF. 1996. *New Astron.* 1:1

Fall SM, Charlot S, Pei YC. 1996. *Ap. J. Lett.* 464:L43

Fasano G, Cristiani S, Arounts S, Filippi M. 1998. *Astron. J.* 115:1400

Fasano G, Filippi M. 1998. *Astron. Astrophys. Suppl.* 129:583

Ferguson HC.1998a. *Reviews in Modern Astronomy* 11:83

Ferguson HC. 1998b. In *The Hubble Deep Field*, ed. M Livio, SM Fall, & P Madau, p. 181. Cambridge: Cambridge University Press

Ferguson HC. 1999. In *Photometric Redshifts and the Detection of High-Redshift Galaxies*, ed. R Weymann, L Storrie-Lombardi, M Sawicki, & R Brunner, p. 51. San Francisco: ASP

Ferguson HC, Babul A. 1998. *MNRAS* 296: 585

Ferguson HC, Baum SA, Brown TM, Busko I, Carollo M, et al. 2000, in preparation

Ferguson HC, McGaugh SS. 1995. *Ap. J.* 440:470

Fernández-Soto A, Lanzetta KM, Yahil A. 1999. *Ap. J.* 513:34

Fixsen DJ, Dwek E, Mather JC, Bennett CL, Shafer R. 1998. *Ap. J.* 508:123

Flores H, Hammer F, Desert FX, Césarsky C, Thuan TX, et al. 1999a. *Astron. Astrophys.* 343:389

Flores H, Hammer F, Thuan TX, Césarsky C, Desert FX, et al. 1999b. *Ap. J.* 517:148

Flynn C, Gould A, Bahcall JN. 1996. *Ap. J. Lett.* 466:L55

Fomalont EB, Kellerman KI, Richards EA, Windhorst RA, Partridge RB. 1997. *Ap. J.* 475:5

Fontana A, D'Odorico S, Fosbury R, Giallongo E, Hook R, et al. 1999. *Astron. Astrophys.* 343:L19

Forbes DA, Phillips AC, Koo DC, Illingworth GD. 1996. *Ap. J.* 462:89

Franceschini A, Silva L, Fasano G, Granato GL, Bressan A, et al. 1998. *Ap. J.* 506:600

Fruchter A, Bergeron LE, Dickinson M, Ferguson HC, Hook RN, et al. 2000, in preparation

Fruchter A, Hook R. 1997. astro-ph/9708242

Fukugita M, Yamashita K, Takahara F, Yoshii Y. 1990. *Ap. J.* 361:L1

Gallego J, Zamorano J, Aragon-Salamanca A, Rego M. 1995. *Ap. J. Lett.* 455:L1

Gardner JP, Baum SA, Brown TM, Carollo CM, Christensen J, et al. 2000. *Astron. J.* 119: 486

Gardner JP, Sharples RM, Frenk CS, Carrasco BE. 1997. *Ap. J.* 480:99

Gardner JP, Cowie LL, Wainscoat RJ. 1993. *Ap. J. Lett.* 415:L9

Gardner JP, Sharples RM, Carrasco BE, Frenk CS. 1996. *MNRAS* 282:L1

Giallongo E, D'Odorico S, Fontana A, Cristiani S, Egami E, et al. 1998. *Astron. J.* 115:2169

Giavalisco M, et al. 2000, in preparation

Giavalisco M, Livio M, Bohlin RC, Macchetto FD, Stecher TP. 1996. *Astron. J.* 112:369

Giavalisco M, Steidel CC, Adelberger KL, Dickinson ME, Pettini M, Kellogg M. 1998. *Ap. J.* 492:428

Gilliland RL, Nugent PE, Phillips MM. 1999. *Ap. J.* 521:30
Gilliland RL, Phillips MM. 1998. *IAU Circular* 6810
Glazebrook K, et al. 2000, in prepraration
Glazebrook K, Ellis RS, Santiago B, Griffiths RE. 1995. *MNRAS* 275:L19
Goldschmidt P, Oliver SJ, Serjeant SB, Baker A, Eaton N, et al. 1997. *MNRAS* 289:465
Goudfrooij P, Gorgas J, Jablonka P. 1999. astro-ph/9910020
Gould A, Bahcall JN, Flynn C. 1996. *Ap. J.* 465:759
Gould A, Bahcall JN, Flynn C. 1997. *Ap. J.* 482:913
Griffiths R, Ratnatunga KU, Casertano S, Im M, Neuschaefer LW, et al. 1996. In *IAU Symposium 168: Examining the Big Bang and Diffuse Background Radiations*, ed. M Kafatos & Y Kondo. Dordrecht: Kluwer
Groth EJ, Peebles PJE. 1977. *Ap. J.* 217:385
Guhathakurta P, Tyson JA, Majewski SR. 1990. *Ap. J. Lett.* 359:L9
Guiderdoni B, Rocca-Volmerange B. 1990. *Astron. Astrophys.* 227:362
Guzman R, Gallego J, Koo DC, Phillips AC, Lowenthal JD, et al. 1997. *Ap. J.* 489:559
Gwyn SDJ, Hartwick FDA. 1996. *Ap. J. Lett.* 468:L77
Haiman Z, Madau P, Loeb A. 1999. *Ap. J.* 514:535
Hansen BMS. 1998. *Nature* 394:860
Hansen BMS. 1999. *Ap. J.* 520:680
Harris H, Dahn CC, Vrba FJ, Henden AA, Liebert J, et al. 1999. astro-ph/9909065
Hauser MG, Arendt RG, Kelsall T, Dwek E, Odegard N, et al. 1998. *Ap. J.* 508:25
Hibbard JE, Vacca WD. 1997. *Astron. J.* 114:1741
Hogg DW, Blandford R, Kundic T, Fassnacht CD, Malhotra S. 1996. *Ap. J.* 467:73
Hogg DW, Cohen JG, Blandford R, Gwyn SDJ, Hartwick FD, et al. 1998. *Astron. J.* 115:1418
Holtzman JA, Burrows CJ, Casertano S, Hester JJ, Trauger JT, et al. 1995. *Publ. Astron. Soc. Pac.* 107:1065
Hornschemeier AE, Brandt WN, Garmire GP, Schneider DP, Broos PS, et al. 2000. *Ap. J.* In press
Hu E, Cowie LL, McMahon RG. 1998. *Ap. J. Lett.* 502:L99
Huang JS, Cowie LL, Gardner JP, Hu EM, Songaila A, Wainscoat RJ. 1997. *Ap. J.* 476:12
Hudson MJ, Gwyn SDJ, Dahle H, Kaiser N. 1998. *Ap. J.* 503:531
Hughes DH, Serjeant S, Dunlop J, Rowan-Robinson M, Blain A, et al. 1998. *Nature* 394:241
Ibata R, Richer HB, Gilliland RL, Scott D. 1999. *Ap. J. Lett.* 524:L95
Im M, Griffiths RE, Naim A, Ratnatunga KU, Roche N, et al. 1999. *Ap. J.* 510:82
Im M, Griffiths RE, Ratnatunga KU, Sarajedini VL. 1996. *Ap. J.* 461:L79
Jain B. 1997. *MNRAS* 287:687
Jarvis RM, MacAlpine G. 1998. *Astron. J.* 116:2724
Karachentsev ID, Makarov DI. 1997. In *IAU Symposium 186: Galaxy Interactions at Low and High Redshift*, ed. JE Barnes & DB Sanders. Dordrecht: Kluwer
Kauffmann G, Charlot S, White SDM. 1996. *MNRAS* 283:L117
Kauffmann G, Colberg JM, Diaferio A, White SDM. 1999. *MNRAS* 307:529
Kauffmann G, White SDM, Guiderdoni B. 1993. *MNRAS* 264:201
Kawaler S. 1998. In *The Hubble Deep Field*, ed. M Livio, SM Fall, & P Madau, p. 353. Cambridge: Cambridge University Press
Kawaler SD. 1996. *Ap. J.* 467:397
Kerins EJ. 1997. *Astron. Astrophys.* 328:5
Kodama T, Bower RG, Bell EF. 1999. *MNRAS* 306:561
Koo DC, Gronwall C, Bruzual GA. 1993. *Ap. J. Lett.* 415:L21
Kron RG. 1980. *Ap. J. Suppl.* 43:305
Landolt AU. 1973. *Astron. J.* 78:959
Landolt AU. 1983. *Astron. J.* 88:439
Landolt AU. 1992a. *Astron. J.* 104:72
Landolt AU. 1992b. *Astron. J.* 104:340
Lanzetta KM, Chen HW, Fernández-Soto A,

Pascarelle S, Puetter R, et al. 1999. In *Photometric Redshifts and the Detection of High-Redshift Galaxies*, ed. R Weymann, L Storrie-Lombardi, M Sawicki, & R Brunner, p. 229., San Francisco: ASP
Lanzetta KM, Wolfe AM, Turnshek DA.1995. *Ap. J.* 440:435
Lanzetta KM, Yahil A, Fernández-Soto A. 1996. *Nature* 381:759
Lanzetta KM, Yahil A, Fernández-Soto A. 1998. *Astron. J.* 116:1066
Larson RB. 1974. *MNRAS* 166:585
Lilly S, Tresse L, Hammer F, Crampton D, Le Fevre O. 1995a. *Ap. J.* 455:108
Lilly SJ, Cowie LL, Gardner JP. 1991. *Ap. J.* 369:79
Lilly SJ, Le Fevre O, Crampton D, Hammer F, Tresse L. 1995b. *Ap. J.* 455:50
Lilly SJ, Le Févre O, Hammer F, Crampton D. 1996. *Ap. J. Lett.* 460:L1
Livio M, Fall SM, Madau P. 1997. *The Hubble Deep Field. Cambridge: Cambridge Univ. Press*
Loveday J, Peterson BA, Efstathiou G, Maddox S. 1992. *Ap. J.* 390:338
Lowenthal JD, Koo DC, Guzman R, Gallego J, Phillips AC, et al. 1997. *Ap. J.* 481:673
Lucas R, Baum SA, Brown TM, Casertano S, de Mello D, et al. 2000, in preparation
Madau P. 1997. In *Star Formation Near and Far*, ed. SS Holt & LG Mundy, p. 481. Woodbury, NY: AIP Press
Madau P, Della Valle M, Panagia N. 1998. *MNRAS* 297:L17
Madau P, Ferguson HC, Dickinson M, Giavalisco M, Steidel CC, Fruchter AS. 1996. *MNRAS* 283:1388
Madau P, Pozzetti L. 1999. astro-ph/9907315
Madau P, Pozzetti L, Dickinson M. 1998. *Ap. J.* 498:106
Magliocchetti M, Bagla JS, Maddox SJ, Lahav O. 1999. astro-ph/9902260
Magliocchetti M, Maddox SJ. 1999. *MNRAS* 306:988
Mann R, Oliver SJ, Serjeant SB, Rowan-Robinson M, Baker A, et al. 1997. *MNRAS* 289:482
Mannucci F, Ferrara A. 1999. *MNRAS* 305:L55
Mao S, Mo HJ. 1998. *MNRAS* 296:847
Maoz D. 1997. *Ap. J. Lett.* 490:L135
Marleau FR, Simard L. 1998. *Ap. J.* 507:585
Marzke RO, Da Costa LN, Pellegrini PS, Willmer CNA, Geller MJ. 1998. *Ap. J.* 503:617
Marzke RO, Geller MJ, Huchra JP, Corwin HG, Jr. 1994. *Astron. J.* 108:437
Matarrese S, Coles P, Lucchin F, Moscardini L. 1997. *MNRAS* 286:115
Matsumoto T, Akiba M, Murakami H. 1988. *Ap. J.* 332:575
McCracken HJ, Metcalfe N, Shanks T, Campos A, Gardner JP, Fong R. 2000. *MNRAS* 311:707
McLeod BA, Rieke MJ. 1995. *Ap. J.* 454:611
Menanteau F, Ellis RS, Abraham RG, Barger AJ, Cowie LL. 1999. *MNRAS* 309:208
Mendez RA, Guzman R. 1997. *Astron. Astrophys.* 333:106
Mendez RA, Minnitti D, Di Marchi G, Baker A, Couch WJ. 1996. *MNRAS* 283:666
Mendez RA, Minniti D. 1999. astro-ph/9908330
Metcalfe N, Shanks T, Campos A, Fong R, Gardner JP. 1996. *Nature* 383:236
Meurer GR, Heckman TM, Calzetti D. 1999. *Ap. J.* 521:64
Meurer GR, Heckman TM, Lehnert MD, Leitherer C, Lowenthal J. 1997. *Astron. J.* 110: 54
Minezaki T, Kobayashi Y, Yoshii Y, Peterson BA. 1998. *Ap. J.* 494:111
Miralles JM, Pello R. 1998. astro-ph/9801062
Mo H, Fukugita M. 1996. *Ap. J. Lett.* 467:L9
Mo H, White SDM. 1996. *MNRAS* 282:347
Mobasher B, Rowan-Robinson M, Georgakakis A, Eaton N. 1996. *MNRAS* 282:L7
Moessner R, Jain B, Villumsen JV. 1998. *MNRAS* 294:291
Moscardini L, Coles P, Lucchin F, Matarrese S. 1998. *MNRAS* 299:95
Moustakas LA, Davis M, Graham JR, Silk J, Peterson BA, Yoshii Y. 1997. *Ap. J.* 475:455
Mushotzky R, Loewenstein M. 1997. *Ap. J. Lett.* 481:L63

Mutz SB, Windhorst RA, Schmidtke PC, Pascarelle SM, Griffiths RE, et al. 1994. *Ap. J.* 434:L55
Muxlow TWB, Wilkinson PN, Richards AMS, Kellerman KI, Richards EA, Garrett MA. 1999. *New Astronomy Reviews* 43:623
Odewahn SC, Windhorst RA, Driver SP, Keel WC. 1996. *Ap. J. Lett.* 472:L13
Ogawa T, Roukema BF, Yamashita K. 1997. *Ap. J.* 484:53
Oke JB. 1974. *Ap. J. Suppl.* 27:21
Oliver SJ, et al. 2000, in preparation
Oliver SJ, Goldschmidt P, Franceschini A, Serjeant SBG, Efstathiou A, et al. 1997. *MNRAS* 289:471
Outram PJ, Boyle BJ, Carswell RF, Hewett PC, Williams RE, Norris RP. 1999. *MNRAS* 305:685
Pain R, Hook IM, Deustua S, Gabi S, Goldhaber G, et al. 1996. *Ap. J.* 473:356
Peacock JA, Rowan-Robinson M, Blain AW, Dunlop JS, Efstathiou A, et al. 1999, submitted
Pei YC, Fall SM. 1995. *Ap. J.* 454:69
Pei YC, Fall SM, Hauser MG. 1999. *Ap. J.* 522:604
Perlmutter S, Aldering G, Goldhaber G, Knop RA, Nugent P, et al. 1999. *Ap. J.* 517:565
Petitjean P, Srianand R. 1999. *Astron. Astrophys.* 345:73
Pettini M, Kellogg M, Steidel CC, Dickinson M, Adelberger KL, Giavalisco M. 1998. *Ap. J.* 508:539
Phillips AC, Guzman R, Gallego J, Koo DC, Lowenthal JD, et al. 1997. *Ap. J.* 489:543
Pozzetti L, Madau P, Zamorani G, Ferguson H, Bruzual G. 1998. astro-ph/9803144
Prantzos N, Silk J. 1998. *Ap. J.* 507:229
Prochaska JX, Burles SM. 1999. *Astron. J.* 117:1957
Puget JL, Abergel A, Bernard JP, Boulanger F, Burton WB, et al. 1996. *Astron. Astrophys.* 308:L5
Reid IN, Yan L, Majewski S, Thompson I, Smail I. 1996. *Astron. J.* 112:1472
Renzini A. 1997. *Ap. J.* 488:35
Renzini A. 1999. In *The Formation of Bulges*, ed. CM Carollo, HC Ferguson, & RFG Wyse, p. 9. New York: Cambridge Univ. Press
Richards EA. 2000. *Ap. J.* In press
Richards EA, Fomalont EB, Kellerman KI, Windhorst RA, Partridge RB, et al. 1999. *Ap. J. Lett.* 526:L73
Richards EA, Kellerman KI, Fomalont EB, Windhorst RA, Partridge RB. 1998. *Astron. J.* 116:1039
Riess A, Filippenko AV, Challis P, Clocchiatti A, Diercks A, et al. 1998. *Astron. J.* 116:1009
Rigopoulou D, Fraceschini A, Genzel R, van der Werf P, Aussel H, et al. 2000. In "*ISO Surveys of a Dusty Universe*," ed. D Lemke, M Stickel, K Wilke, in press. astro-ph/9912544
Rigopoulou D, Spoon HWW, Genzel R, Lutz D, Moorwood AFM, Tran QD. 1999. astro-ph/9908300
Rix HW, Guhathakurta P, Colless M, Ing K. 1997. *MNRAS* 285:779
Roche N, Ratnatunga K, Griffiths RE, Im M, Naim A. 1998. *MNRAS* 293:157
Roukema BF, Valls-Gabaud D. 1997. *Ap. J.* 488:524
Roukema BF, Valls-Gabaud D, Mobasher B, Bajtlik S. 1999. astro-ph/9901299
Rowan-Robinson M. 1999. astro-ph/9906308
Rowan-Robinson M, Mann RG, Oliver SJ, Efstathiou A, Eaton N, et al. 1997. *MNRAS* 289:490
Ruiz-Lapuente P, Canal R. 1998. *Ap. J. Lett.* 497:L57
Sahu K. 1994. *Nature* 370:275
Salpeter EE. 1955. *Ap. J.* 121:161
Sandage A. 1961. *Ap. J.* 133:355
Sandage A. 1988. *Annu. Rev. Astron. Astrophys.* 26:561
Sandage A. 2000. Preprint
Savaglio S. 1998. *Astron. J.* 116:1055
Savaglio S, Ferguson HC, Brown TM, Espey BR, Sahu KC, et al. 1999. *Ap. J. Lett.* 515:L5
Sawicki M, Yee HKC. 1998. *Ap. J.* 115:1329
Sawicki MJ, Lin H, Yee HKC. 1997. *Astron. J.* 113:1
Scalo JM. 1986. *Fundam. Cosmic Phys.* 11:1
Schade D, Lilly SJ, Crampton D, Ellis RS, Le Fevre O, et al. 1999. *Ap. J.* 525:31

Schade D, Lilly SJ, Crampton D, Hammer F, Le Fevre O, Tresse L. 1995a. *Ap. J. Lett.* 451:L1
Schade D, Lilly SJ, Crampton D, Hammer F, Le Fevre O, Tresse L. 1995b. *Ap. J. Lett.* 451:L1
Schechter P. 1976. *Ap. J.* 203:297
Sealey KM, Drinkwater MJ, Webb JK. 1998. *Ap. J. Lett.* 499:L135
Serjeant SBG, Eaton N, Oliver SJ, Efstathiou A, Goldschmidt P, et al. 1997. *MNRAS* 289: 457
Simard L, Koo DC, Faber SM, Sarajedini VL, Vogt NP, et al. 1999. *Ap. J.* 519:563
Simard L, Pritchet C. 1998. *Ap. J.* 505:96
Smail I, Ivison RJ, Blain AW. 1997. *Ap. J. Lett.* 490:L5
Spinrad H, Stern D, Bunker A, Dey A, Lanzetta K, et al. 1998. *Astron. J.* 116:2617
Spinrad H, Stone RPS. 1978. *Ap. J.* 226:609
Stanford SA, Eisenhardt PR, Dickinson M. 1995. *Ap. J.* 450:512
Stanford SA, Eisenhardt PR, Dickinson M. 1998. *Ap. J.* 492:461
Steidel CC, Adelberger KL, Dickinson M, Giavalisco M, Pettini M, Kellogg MA. 1998. *Ap. J.* 492:428
Steidel CC, Adelberger KL, Giavalisco M, Dickinson M, Pettini M. 1999. *Ap. J.* 519:1
Steidel CC, Giavalisco M, Dickinson M, Adelberger KL. 1996. *Astron. J.* 112:352
Steidel CC, Pettini M, Hamilton D. 1996. *Astron. J.* 110:2519
Stiavelli M, Treu M, Carollo CM, Rosati P, Viezzer R, et al. 1999. *Astron. Astrophys.* 343:L25
Tanvir NR, Aragón-Salamanca A, Wall JV. 1996. *The Hubble Space Telescope and the High Redshift Universe* Singapore: World Scientific
Teplitz H, Gardner J, Malmuth E, Heap S. 1998. *Ap. J. Lett.* 507:L17
Thompson RI. 1999. In *Photometric Redshifts and High Redshift Galaxies*, ed. RJ Weymann, LJ Storrie-Lombardi, M Sawicki, & RJ Brunner, p. 51. San Francisco: ASP
Thompson RI, Storrie-Lombardi LJ, Weymann RJ, Rieke MJ, Schneider, G, et al. 1999. *Astron. J.* 117:17
Tinsley BM. 1978. *Ap. J.* 220:816
Tinsley BM, Gunn J. 1976. *Ap. J.* 302:52
Tosi M. 1996. In *From Stars to Galaxies: The Impact of Stellar Physics on Galaxy Evolution, ASP conf. ser. 98*, ed. C Leitherer, U Fritze-von-Alvensleben, & J Huchra, p. 299. San Francisco: ASP
Totani T, Yoshii Y. 1998. *Ap. J. Lett.* 501:L177
Trentham N, Kormendy J, Sanders DB. 1999. *Ap. J.* 117:2152
Tresse L, Dennefeld M, Petitjean P, Cristiani S, White SDM. 1999. *Astron. Astrophys.* 346:L21
Treu M, Stiavelli M. 1999. *Ap. J. Lett.* 524:L27
Treu M, Stiavelli M, Casertano S, Møller P, Bertin G. 1999. *MNRAS* 308:1037
Treu M, Stiavelli M, Walker AR, Williams RE, Baum SA, et al. 1998. *Astron. Astrophys.* 340:L10
Tyson JA. 1988. *Astron. J.* 96:1
Tyson JA, Jarvis JF. 1979. *Ap. J.* 230:L153
van den Bergh S, Abraham RG, Ellis RS, Tanvir NR, Santiago BX, Glazebrook K. 1996. *Astron. J.* 112:359
van Dokkum P, Franx M, Kelson DD, Illingworth G, Fisher D, Fabricant D. 1998. *Ap. J.* 500:714
Villumsen J, Freudling W, da Costa LN. 1997. *Ap. J.* 481:578
Vogeley M. 1997. astro-ph/9711209
Vogt NP, Forbes DA, Phillips AC, Gronwall C, Faber SM, et al. 1996. *Ap. J.* 465:15
Vogt NP, Phillips AC, Faber SM, Gallego J, Gronwall C, et al. 1997. *Ap. J. Lett.* 479:L121
Waddington I, Windhorst RA, Cohen SH, Partridge RB, Spinrad H, Stern D. 1999. *Ap. J. Lett.* 526:L77
Wang Y, Bahcall N, Turner EL. 1998. *Astron. J.* 116:208
Weymann RJ, Stern D, Bunker A, Spinrad H, Chaffee FH, et al. 1998. *Ap. J.* 505:95
White SDM, Frenk CS. 1991. *Ap. J.* 379:52
Whitmore B, Heyer I, Casertano S. 1999. *Publ. Astron. Soc. Pac.* 111:1559

Williams RE, Baum SA, Bergeron LE, Bernstein N, Blacker BS, et al. 2000, Astron. T. Submitted

Williams RE, Blacker B, Dickinson M, Dixon WVD, Ferguson HC, et al. 1996. *Astron. J.* 112:1335

Wilner D, Wright MCH. 1997. *Ap. J. Lett.* 488:L67

Yahata N, Lanzetta KM, Chen HW, Fernandez-Soto A, Pascarelle S, et al. 2000. *Ap. J.* In press, astro-ph/0003310

Zepf S. 1997. *Nature* 390:377

Zepf SE, Moustakas LA, Davis M. 1997. *Ap. J. Lett.* 474:L1

Zucca E, Pozzetti L, Zamorani G. 1994. *MNRAS* 269:953

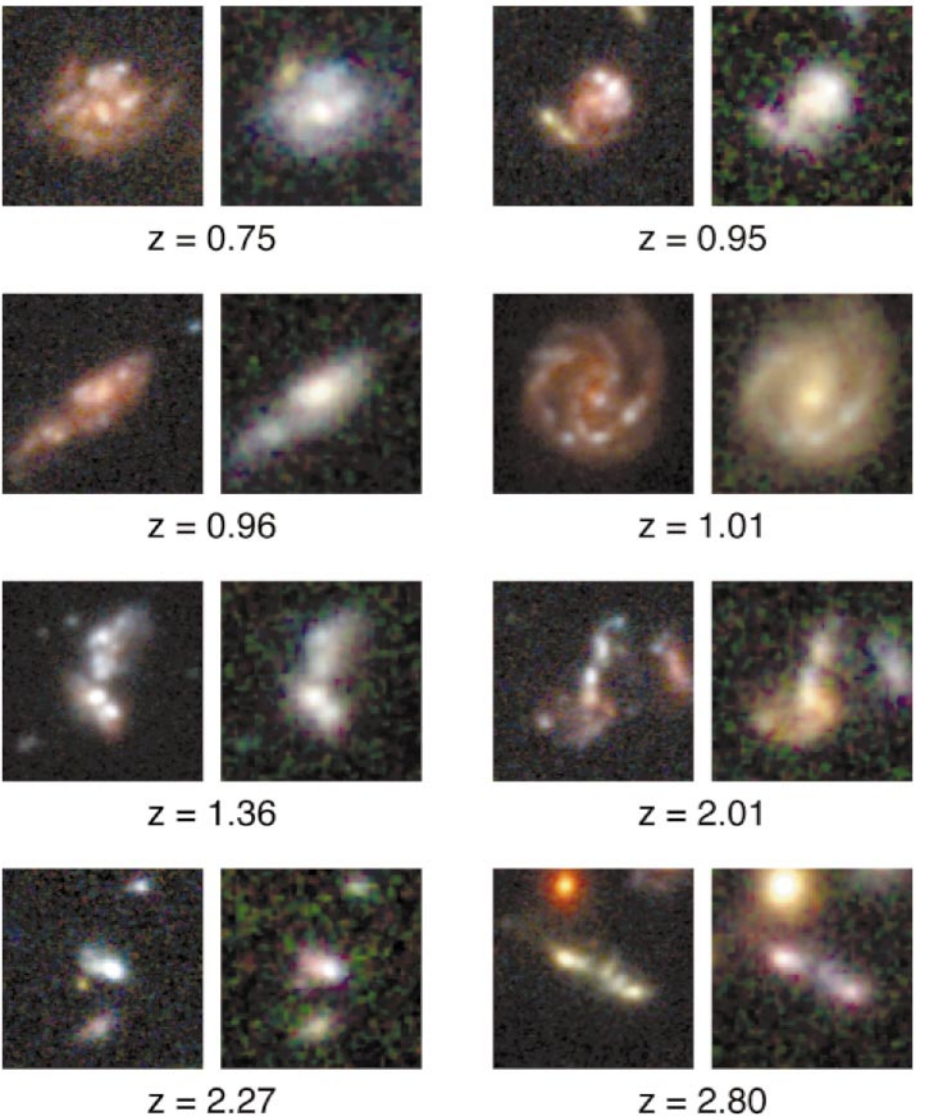

Figure 3 Selected galaxies from the HDF-N, viewed at optical and near-infrared wavelengths with WFPC2 and NICMOS. For each galaxy, the two panels how color composites made from B_{450}, V_{606}, I_{814} (*left*) and I_{814}, J_{110}, H_{160} (*right*). The NICMOS image have omewhat poorer angular resolution. In the giant spiral at $z = 1.01$, a prominent red bulge and bar appear in the NICMOS images, while the spiral arms and HII regions are enhanced in the WFPC2 data. For most of the other objects, including the more irregular galaxies at $z \sim 1$ and the Lyman Break galaxies at $z > 2$, the morphologies are similar in WFPC2 and NICMOS.